Thesis Summary

Three Dimensional Numerical Manifold Method and Rock Engineering Applications

Presented by Dr. He Lei

School of Civil and Environment Engineering

Nanyang Technological University, Singapore

Doctor titled Time: May, 2011

Thesis Summary submission time: December, 2011

To: International Society for Rock Mechanics

Abstract

The numerical manifold method (NMM) is one of most suitable methods to simulate deformations and stabilities of rock masses, as the NMM itself can be thought as a bridge connecting two branches of numerical methods: continuum methods (e.g. FEM) and discontinuum methods (e.g. DDA). Since it was first proposed in 1991, most of research works on the NMM were carried out within the two-dimensional (2-D) framework. However, more advanced numerical method within a three-dimensional framework could be realistic and beneficial to the practicing problems, which is highly demanded in rock engineering.

This thesis extends the numerical manifold method to the 3-D domain based on the 2-D fundamentals.

In ***part 1***, it shortly briefs the importance and necessity to develop the 3-D NMM.

In ***part 2***, the conceptual framework of the 3-D NMM is established, including the definitions of the mathematical cover, physical cover, manifold pattern and manifold element in the 3-D domain.

In ***part 3***, a new general 3-D contact algorithm is subsequently developed for the 3-D NMM. The proposed contact treatment procedure consists of distinct features, which equip 3-D NMM with an efficient and accurate strategy of contact treatment. It proposes three operation phases for the checking process, NMM hierarchical contact system, pre-warning subroutine based on mathematical patterns (*MP*s), transforming measures for two essential entrance modes, post-transferring contact information function, penalty treatment for contact constraints, open-closed iteration process, and lagged verification on contact state.

In ***part 4***, verification examples of the 3-D NMM are tested. The scenario of "*free fall of a block*", "*mesh size effect*" and "*mesh orientation effect*" are designed to test the ability to model continuous problems of the proposed 3-D NMM. The "*sliding cube on an inclined plane*", "*roof wedge falling*", and "*Tetrahedral wedge sliding*" are designed to test for discontinuous problems, and "*3-D dominos run*" and "*dougong/brackets structure*" are designed for robust test in multi-blocky system.

Slope and tunnels in jointed rock mass are two typical difficulties; therefore ***part 5*** specifically addresses stability analysis of two scenarios in rock engineering, i.e., stability analysis of rock slopes and tunnels by the proposed 3-D NMM.

In ***part 6***, it concludes the robustness, efficiency, and stableness of the proposed 3-D NMM, which are equipped with both static and dynamic function. It has great potential to be further developed and applied in practical rock engineering.

Keywords*:* 3-D Numerical Manifold Method (NMM), 3-D contact algorithm, 3-D manifold patterns, discontinuous deformation, dynamic analysis, rock slope & tunnel.

Part 1: Introduction

Prevalent geologic hazards have caused various catastrophic damage and fatality in the global infrastructure development. More profound understanding to such geotechnical problems is necessary to reduce the disastrous damage in rock structures.

Rock masses, generated in the natural environment, are complex with stochastic uncertainties and imperfections to different extent. These imperfections are displayed as bedding planes, joints, shear zones and faults, which make the rock mass to be a combined solid of continuum and discontinuum. The distinct feature of the rock masses creates tremendous difficulties in the analysis procedure.

In the earlier stage, geotechnical engineering problems were usually analyzed by theoretical approaches through differential equations with specified boundary conditions. However, most close-form theoretical solutions nominally over-simplify the pragmatic problem, and they are more suitable to the continuous structure, although theoretical methods provide basic formations and foundations. The second approach to understand rock mass is the laboratory tests, which could provide informative evaluation, however, it might be expensive and incomplete.

Numerical methods, as a way to complement to other approaches, provide potential solutions to relative complicate problems.

The finite element method (FEM) and finite difference method (FDM) are very well developed and have been widely applied in various engineering analysis, but both methods in the rock related field extended the over-simplifying the local and global influence of the joint network in rock masses. They inherit the assumption of small displacement/deformation from the theoretical method, and the complex mathematical troubles encountered in meshing and re-meshing processes reduce the

efficiency and accuracy. A variety of mesh-free and node-based methods have recently been proposed to overcome problems such as "meshing trouble". The application of these methods is yet limited by boundary treatments especially for contact and multi-physical problems with intensive computational cost.

On the other hand, FEM and FDM are initially brought up in the framework of continuum mechanics. In order to extend their applicability to multi-body, heterogeneous structure and jointed solids, the interface elements or "*slide lines*"(Goodman et al., 1968) have been put forward, which enables them to model a discontinuous material. However, their application are restricted in many aspects, e.g. multi-intersecting interface cases, new contact detection in complex media or larger displacement between. A better solution related to problems with jointed rock mass is the distinct element method (Cundall, 1971) or the discontinuous deformation analysis (DDA)(Shi, 1988).

Among numerous numerical methods, the numerical manifold method (NMM) (Shi, 1997; Shi, 1991) was treated as a combination of the finite element method (FEM, a continuum-based method) and the discontinuous deformation analysis (DDA, a discontinuum-based method) method. It makes NMM quite suitable for rock analysis.

The bridging between the FEM and the DDA is achieved through a fundamental concept of covers (including mathematical and physical covers) under the NMM framework. The terminology "*manifold*" comes from the topological manifold and differential manifold, which is the main subject of differential geometry, algebraic topology, differential topology and modern algebra of mathematics (Shi, 1996). Manifold is mathematically defined when a function is continuous and differentiable at each cover in the description domain and all covers are independent. The overlapping mathematical covers create various manifold elements through intersecting with the physical domain which generates the continuous and differentiable function description in the whole domain. They are the advantages that make NMM applicable to a blocky system or a cracked system with dense discontinuities in the domain since the NMM inherits the merits of the DDA. As the preparation of mathematical cover is independent of physical domain, the geometrical shape can be user-defined freely. Each mathematical cover does not require conforming to the boundaries of its structure. It is also able to remarkably reduce the workload in processing the meshes of tedious jointed masses. Furthermore, it prompts a new idea for multi-physical modeling by introducing more layers of mathematical meshes.

Part 2: 3-D Numerical Manifold Method

Part 2-A: History and Basic theory of Numerical Manifold Method

The basic concepts consist of three major parts: finite cover system, simplex integration and block kinematics.

Firstly, the *finite cover system* divided a problem into two independent cover systems, i.e., a physical cover system in the physical/material domain and a mathematical cover system in the manifold/mathematical domain. The physical covers consisted of a blocky system which provided physical information, such as boundaries of the blocks, joints, and the interfaces of different material zones, etc. The mathematical covers would control the precision level of approximation to the unknown functions. The covers in the mathematical domain were defined according to the geometry of the concerned problem, accuracy requirement and physical zones. At the first stage of preprocessing, the mathematical covers rebuilt the physical block system with sub-blocks. In the second stage, the sub-block system brought back the geometric information to the mathematical covers to construct the manifold element system.

In manifold computation, the mathematical cover system and physical cover system were independent. Therefore, mathematical covers were free to be defined and their size and shape were free to change. The mathematical covers could be deformed, split and even removed. Large deformations and moving boundaries could be computed through allocating the mathematical covers. The joints and block boundaries divide a cover into two or more independent covers together with the dedicated displacement functions, thus the general discontinuous materials is modeled.

Secondly, the "*Simplex integration method*" was adopted in the NMM computation. An arbitrary 2-D domain of integration to a function was converted into many triangles. Integration was done based on these triangles, which helped to ensure high precision analytically (Li et al., 2005)

The third basic concept is the block kinematics. 2-D NMM inherited contact detection techniques and the block kinematics from the DDA contact algorithm. The contact detection algorithm was described by inequalities (Shi, 1988). The kinematics for material was based on the contact theory. The discontinuous

displacements were computed via searching the contacts in each time step and applying stiff springs on detected contact zones. It had been realized that the contact algorithm migrated into the 2-D NMM is effective and accurate.

It has specific interpretation on some concepts such as “Manifold”, “Physical domain”, “Mathematical domain”, “Target Physical objects”, “Initial mathematical mesh”, “Mathematical cover (MC)”, “Physical cover (PC)”, “Manifold star”, “Manifold element (ME)”, “Manifold pattern (MP)”, “Loop/Contact surface”, “Cover function”, “Weight function”, “Simplex integration”, and “Discontinuity” (*Detailed information on the Nomenclature, refer to Section 3.1.1 in the thesis*). The procedure of NMM (for both 2-D and 3-D) refers to thesis figure “General procedure of NMM”. Fig. 2-1 illustrates the interaction process. A manifold pattern system and a discrete material domain (MEs) are generated.

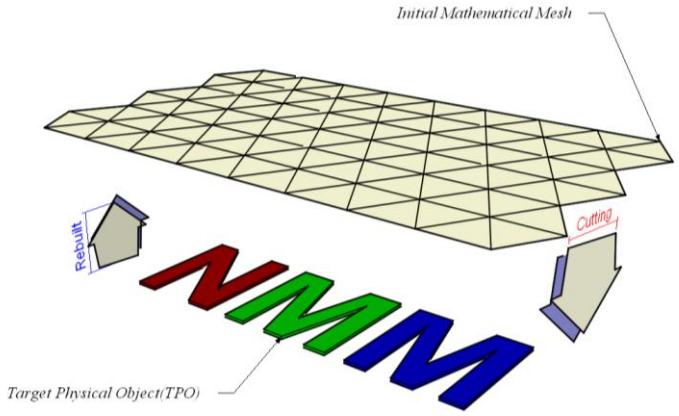

(a) Pre-process

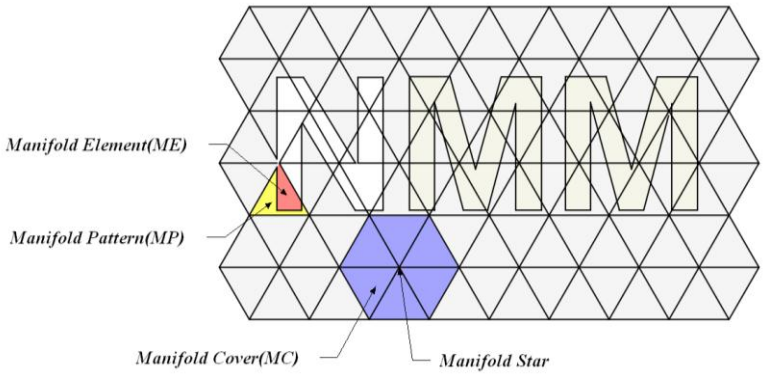

(b) Definition of manifold system

Figure 2- 1 Illustration of NMM procedure

2-D NMM has been extended in various direction such as through higher order cover functions to improve the accuracy, applying it to discontinuous implementation (e.g., crack initiation, propagation and shear failures), and developing of Eulerian NMM. Besides, NMM had been applied to simulate other problems, such as saturated/

unsaturated unsteady groundwater flow analysis, rock masses containing joints of two different scales, data compression, dynamic non-linear analysis of saturated porous media, the shear response of heterogeneous rock joints, dynamic friction mechanism of blocky rock system, fluid-solid interaction analysis, plane micropolar elasticity study, and multiple discrete blocks (*Detailed literatures refer to thesis section 2.3*).

The 2-D NMM has already been widely proven by abundant examples, however, the real problems in practice are always in the three dimensional space. Due to the complexity in geometry description and the absence of a reliable 3-D contact algorithm, it has been a long time challenge to raise the NMM for three dimensional analyses. The increasing underground construction and geotechnical works strongly demand for a 3-D discontinuous deformation analysis tool, especially in rock engineering analysis. Some preliminary basic theoretical formulation of 3-D NMM is firstly derived, although the solution is far from engineering practical application (Cheng et al., 2002).

Up till now, there are very few studies performed on the 3-D NMM. Only few literatures focused on the concept extension and equation derivation, and they seemed lack convictive application examples to complete their arguments. The main difficulties are proper preprocessing tools for rock-mass modeling and a contact algorithm for blocky system, which are to be solved toward the 3-D NMM.

Part 2-B: Theory of 3-D numerical Manifold Method

3-D numerical manifold method is inherited from 2-D version, which is based on three important concepts: mathematical cover (*MC*), physical cover (*PC*) and manifold element (*ME*).

Physical domain is used to represent the portrait of target physical objects (*TPO*) in general sense. *TPO*s include all the physical features such as internal discontinuities (e.g. joints, material interfaces and cracks) and external geometries on which boundary conditions are prescribed.

Then, *MC*s intersect and paste seamlessly to re-divide the *TPO*s, during which *PC*s are generated. Further, elements (*ME*s) in the NMM framework can be considered as the common part of overlapping *PC*s. In this way, the NMM can be easily understood and extended to the three dimensional case.

Fig. 2-2 (a) illustrates the three basic concepts of the NMM in a 3-D view. There are two MCs in total, a sphere *MC1* and a hexahedron *MC2*. A pyramid represents the physical domain in this instance. A discontinuity inserts into the pyramid body. Interacting with the physical domain, four *PC*s, as shown in Fig. 2-2 (c), are generated. These PCs finally form five manifold elements as shown in Fig. 2-2 (e). Despite the illustrated sphere and hexahedron MC in Fig. 2-2, one important feature of NMM is that any convex polyhedron in the 3-D space can be decomposed into several tetrahedrons, and the decomposition plans are innumerable (e.g., choosing different block size). The division plan determines the shape of the MCs.

It could have many kinds of tetrahedrons plans (as shown in Fig.2-2(a)). The advantage is that the cube has the property of center-symmetry, and it can build up the entire 3D space without rotation. The two schemes of 5 Tetra-plan (Fig. 2-2(b) and 2-2(c)) are usually coupled and applied as a mixed-discretization (M-D) zone (Itasca Conculting Group, 2003). As these two kinds of mesh are symmetric to each other, they can overlap at the same position to decrease "*the strain instability induced by choosing mesh direction*". One cubic domain and cover is generated by two "*anisotropy*" mathematical covers, which is another extension of the manifold concept. When using the centers of cube and 6 faces as auxiliary points, a cube can be decomposed into 24 different tetrahedrons. The mathematical mesh has extremely symmetrical property by this 24-tetrahedron decomposition scheme.

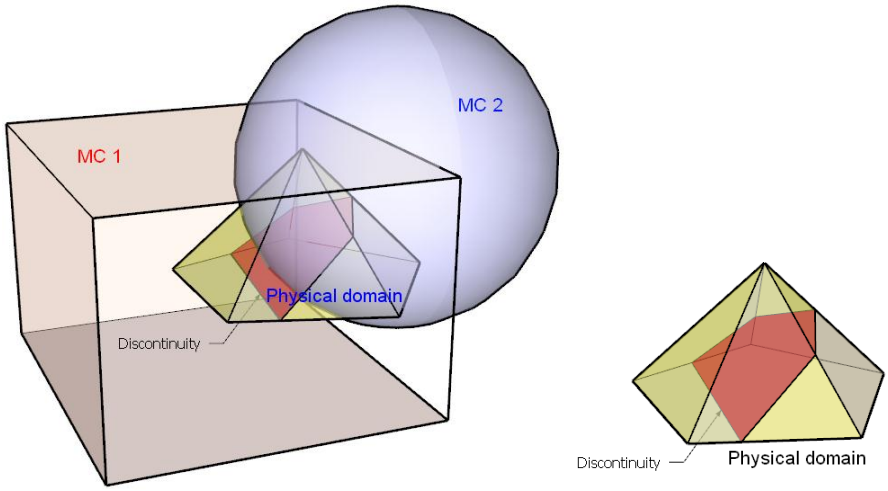

(a) Physical domain and mathematical covers (b) Pyramid with discontinuity (TPOs) in physical domain

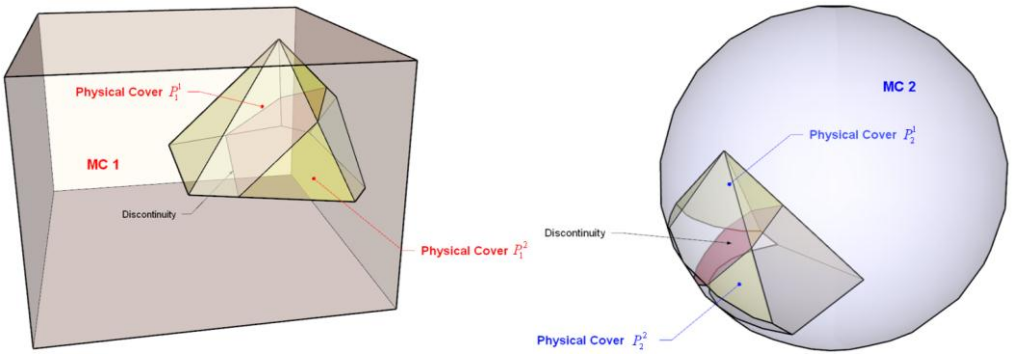

(c) Physical Covers (PCs) with Manifold Covers(MCs)

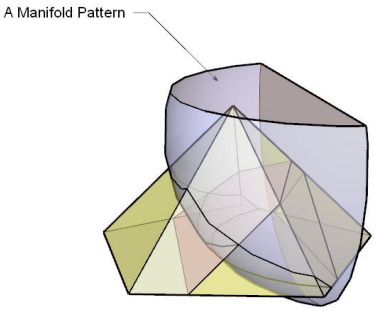

(d) Representation of Manifold Pattern (MP)

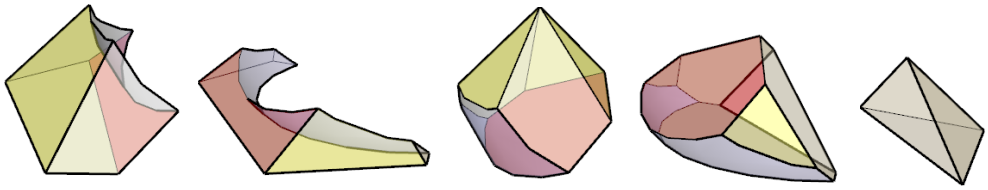

$E(P_1^1)$ $E(P_1^2)$ $E(P_1^1, P_2^1)$ $E(P_1^2, P_2^2)$ $E(P_2^2)$

(e) Manifold Elements (MEs)

Figure 2- 2 Illustration of finite cover system in the 3-D NMM

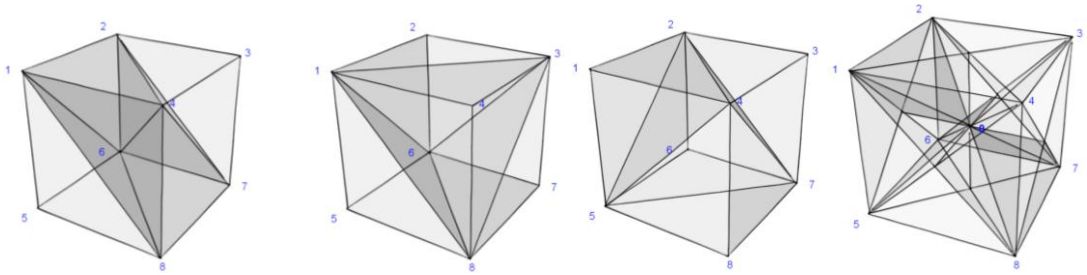

(a) (b) (c) (d)

Figure 2- 3 Decomposition plan from hexahedron to tetrahedron

The geometry structure can be gained after applying the decomposition plan, and weight functions of the covers, cover functions, constant cover function, linear cover function, second-order cover function could be derived in its 3-D version (*Detailed equations refer to section 3.2.3 in the thesis*). Numerically, the general formulations of NMM approximation including the weak form of governing equations, NMM

interpolations, discrete equations, equilibrium equation based on tetrahedral MP, elastic stiffness matrix, inertia term matrix, initial stress matrix, point loading matrix, body force matrix, matrix for displacement boundary point & fixed point and simplex integration for 3-D arbitrary polyhedron are gained (*Equations in 3-D refer to section 3.3 and 3.4 in the thesis*).

Part 3: The 3-D Contact Algorithm

Part 3-A: General Contact Algorithm

Contact algorithm plays a key role in further developing the numerical simulation technique. For example, the extensive development on popular topics (e.g., complex crack propagation and fluid-solid coupling problem) is highly dependent on a reliable contact algorithm. However, contact algorithm has been sealed into commercial software (e.g., LSDYNA, AUTODYN) as a "*black box*". Generally speaking, contact interaction is a special kind of boundary with trigger condition, also called "***contact constraint***", except widely known loading boundary and displacement boundary in continuum mechanics. In other words, we are only required to put additional terms, triggered by contact, into local balance equations based on continuum mechanics. These equations, which describe the behavior of bodies whether coming into contact or not, have not made essential difference.

Boundary conditions can be classified into two groups: 1) ***prescribed boundary conditions*** and 2) ***uncertain boundary conditions***. The prescribed boundary conditions are motion-deformation independent, while the uncertain one is motion-deformation dependent.

Displacment boundary conditions and traction boundary conditions are the typical prescribed boundary conditions. Contact boundary condition is an important branch of uncertain boundary conditions (Detailed basic formulation of the 3-D contact problem and different constitutivemodels describing the contact interface could be referred to thesis section 4.3).

Another important issue is the method on how to warn potential contacting zones and to locate contacting zones reliably and efficiently, which is so-called *contact checking procedure* (searching/detection). Previous contact studies focus on how to implement the contact constraints assuming that the possible contact points are already known (Benson and Hallquist, 1990), as incipient contact problems limit

themselves in simple one-to-one contact cases in 2-D. Their non-complex geo-configuration, non-fine mesh, and less contact body make researchers easy to neglect the importance of "*contact detection*" part in algorithm.

Besides, there are other difficulties which impede its previous developments on the contact checking algorithm. 1) The arbitrary geometries of contact bodies, large displacement, and rotations, which makes contact may occur or disappear at non-predictable places on any contact boundary involved at any time instant, or undergo changeable interface size, locations, and splitting of material masses. 2) A general contact checking algorithm, in principle, is not obligatory to distinguish diverse application areas. For instance, calculation in mechanical engineering (e.g., automobile collapse analysis) involves performing large plastic deformation (crash and buckling). Large deformation will cause complex self-contact issue. Meanwhile rocks in the discontinuous blocky system in geotechnical engineering (e.g., tunnel, excavation, and rock slope) do not undergo large deformation, but large displacement/rotations and un-regular shape itself. 3) The process of contact checking operation is quite expensive in computational cost. Since the total number of contacting pair is unknown prior to the solution of the problem, most of the computation time has to be devoted to searching and checking both for explicit and implicit time integration method. All these contribute the complexity of contact problem. Therefore, suitable algorithm is required to fit different practical applications.

Two well-developed branches of contact checking algorithm from 90s in the last century are: 1) Under continuum mechanics, e.g., FEM, FDM. They focused on large deformation cases (Shell component in automobile design). 2) Under dis-continuum mechanics, e.g., DEM, DDA. They focused on large displacement cases (rock mass in slope or tunneling design). This thesis focuses on developing 3-D NMM under Lagrangian framework. Most approaches developed by later-on researchers are mostly built to balance two methods *MSC* (Master-Slave Contact) having high calculation speed and tedious manual intervention and *SSC* (Single Surface contact) having automatic process but slow calculation speed.

NMM could be seen as a unified method. Its contact checking algorithm is also compatible to both FEM and DDA. In general, locating and tracking the contact zone has been split into *three phases, which* are related to purely geometrical consideration, and only depend on the geometric information of contact bodies. 1) *Contact warning*: spatial search for objects which **might possibly** come into contact; (also called global searching); 2) *Contact detection*: determination of pairs of objects

which **actually intersect** and hence are in contact (also called local searching).(Detailed review on methods used in previous studies refers to thesis section 4.4.2); 3) *Contact transferring*: record the state of each contact pair (open-close/lock sliding situation) for reference to next iteration/time/load step contact checking.

After contact checking procedure of located contacting zones, different strategies could be used to find the maximum/minimum of a function subject to constraints in terms of its numerical treatment, such as the penalty method, the lagrange multiplier method, and he augmented lagrange method, which are widely used in most standard numerical codes (Ansys, Lsdyna, 3DEC, 2-D DDA/NMM).

Part 3-B: The 3-D NMM Contact Mechanics

The contact checking algorithm in proposed 3-D NMM has three phases: warning, detection, transferring. Not all the contact checking algorithm mentioned in the previous section is suitable for the NMM requirement, because of its particular features. In fact, the specific techniques that fit for NMM are not constrained from the classification of Phase I or Phase II discussed in previous chapter. In other words, the function under the Phase II framework can be applied to fulfill the global searching requirement, and vice versa. The discontinuity and random rock mass shape, arbitrary shaped polyhedron of NMM as its manifold element, and implicitly hidden mathematical cell prohibit the direct usage of many contact checking algorithm.

One specific contribution of this thesis is to explore a viable and efficient notion to enable 3-D NMM with handling capacity to contact problem, from these previous works.

The basic idea of 3-D NMM contact checking algorithm is built upon the concept of ***entrance mode***. Inspired by 2-D DDA (Shi, 1988), two entrance modes of the designed 3-D NMM are defined (point-to-plane mode and crossing-line mode), which could transform any of 7 basic contact types (vertex-to-facet, crossing edge-to-edge, parallel edge-to-edge, vertex-to-edge, vertex-to-vertex, edge-to-facet, and facet-to-facet).

The procedure of contact checking algorithm in 3-D NMM is to: locate contact pair candidates→determine contact pair candidates' type→transform into entrance

mode→screen real contact pair and calculate penetration depth→record real contact pair information. They are realized specifically by the bellowing 6 processes.

Step 1: Setup Process

Setup process is to setup contact hierarchies and outer normal vector of hierarchies. The contact system of 3-D NMM are divided into 5 levels, which are contact body, contact manifold element, contact facet, contact edge, and contact vertex. Obviously, a hierarchical relation exists among those ***contact hierarchical objects/contact hierarchies.*** Fig. 3-1 assumes a solid polyhedron as a ***contact body*** is placed in mathematical mesh, and the polyhedron is discretized into many manifold elements according to the NMM definition. There are two kinds of element here. One is internal element, and the other is external element, which is attached by contact boundary surface. The latter one is referred to as "***contact manifold element***". Contact manifold element, itself, is a collection of facet. We define the external facets as ***contact facet***, which are on the contact boundary. Each contact facet is again defined by ***contact edge***. Contact edge normally embodies two ***contact vertexes***.

Step 2: Warning Process

Warning process is to do contact warning with single block generation methodology. If we concentrate to observe mathematical cells in the whole process, it is not hard to find that the responding mathematically cells have already overlapped before the real contact occurs. S***ingle block cutting methodology*** is used (He and Ma, 2010) to detect overlapping cells. Each mathematical cell, say a cube, is formed by a set of six planes. The intersection part of two cells can be considered as a union of two sets of planes, as the vertexes of intersection body must satisfy Half-space requirements for those 12 planes.

Single block cutting methodology can determine the topological expression of union parts, and then use simplex integration formulation to gain the volume of the intersection body. Fig. 3-3 gives the intersection examples of some hexahedron cell pairs.

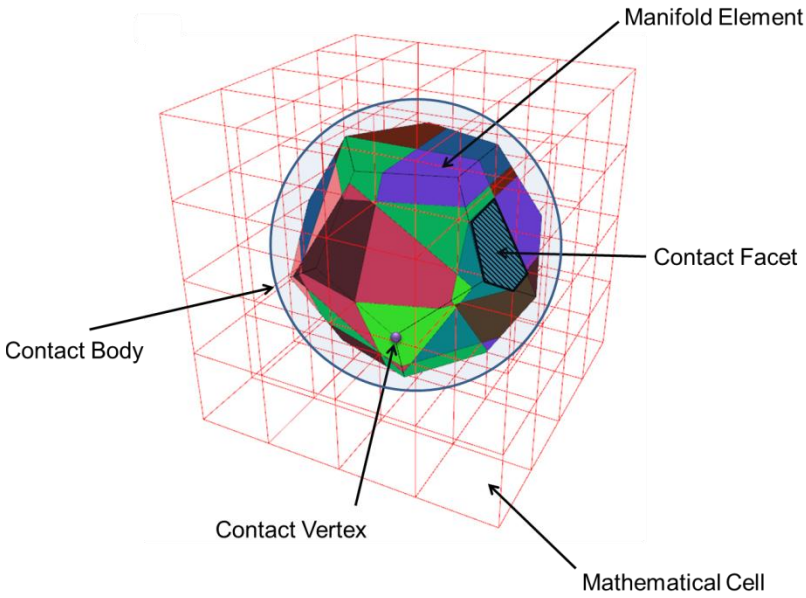

Figure 3- 1 Contact system of 3-D NMM

The tree structure of hierarchical contact system and its referred concepts are depicted in Fig. 3-2.

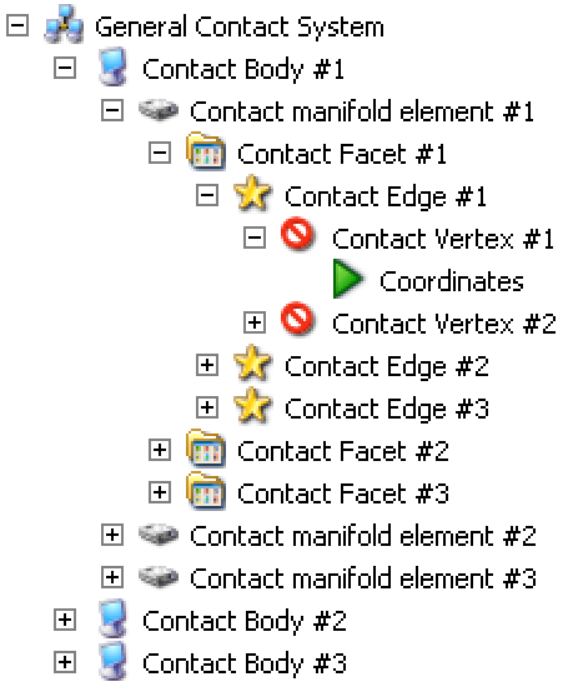

Figure 3- 2 Hierarchical contact system in 3-D NMM

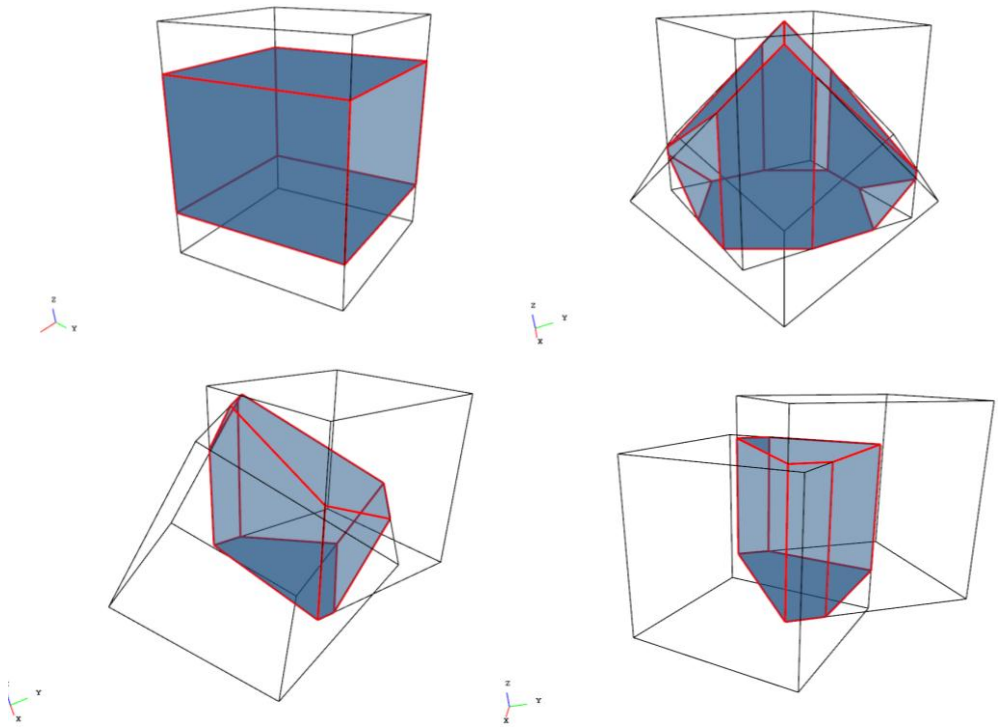

Figure 3- 3 Examples for the intersection body of two mathematical cells

When the value of volume is positive, it indicates that overlapping happens, and contact warning is activated. Under this strategy, we find both contact body pairs and potential contact manifold element pairs. Further contact locating is at the external facet of manifold element and at descendent level of ***primitive hierarchies*** (primitive hierarchies includes facet, edge, vertex), which is the task for next step. From the following steps, contact checking procedure enters Phase II.

Step 3: Matching Process

Matching process is to setup contact territory and match hierarchical contact pair. The definition of the contact territory follows the criterion that all candidate objects approaching the target object will be caught and tested for contact matching before the interpenetration occurring. As shown in Fig. 3-4, Fig. 3-5, Fig. 3-6 (where D_c is the territory expansion, which is controlled by the prescribed maximum relative vertex displacement in a special time step, equivalent to maximum displacement ratio in 2-D NMM.)

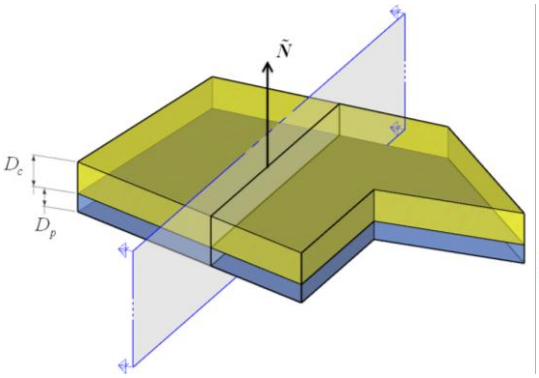

Figure 3- 4 Contact territory of contact facet

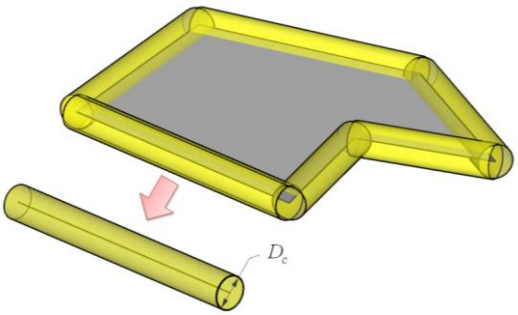

Figure 3- 5 Contact territory of contact edge

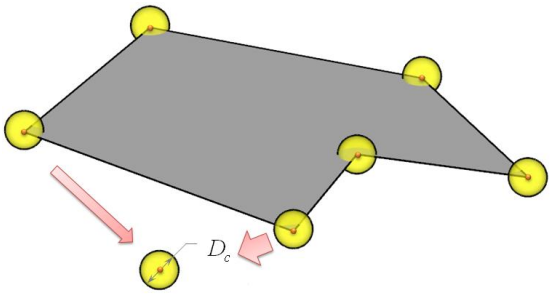

Figure 3- 6 Contact territory of contact vertex

Assisting by territory, we can easily match the primitive hierarchies of contact element pairs. After the matching check guaranteed by territory overlapping detection, ***second matching check*** is designed to avoid possible missing contact pairs. Second matching check is built on the concept of a ***target neighbor***. A target neighbor is a collection of one of primitive contact hierarchies and its neighboring contact facet (including its belongings). Since three primitive contact hierarchies are vertex, edge, and facet. Thus, the target neighbor can be categorized into three groups: the vertex-centered target neighbor, the edge-centered target neighbor, and the facet-centered target neighbor.

Step 4: Transform Process

Transform process is to transform contact pair candidates with essential types to entrance mode. In the reduced four essential contact types as decomposition in previous step, vertex-to-facet and edge-to-edge (crossing) are very easy to handle, and transform to two given entrance modes correspondingly. These two contact pairs have only one entrance mode accordingly.

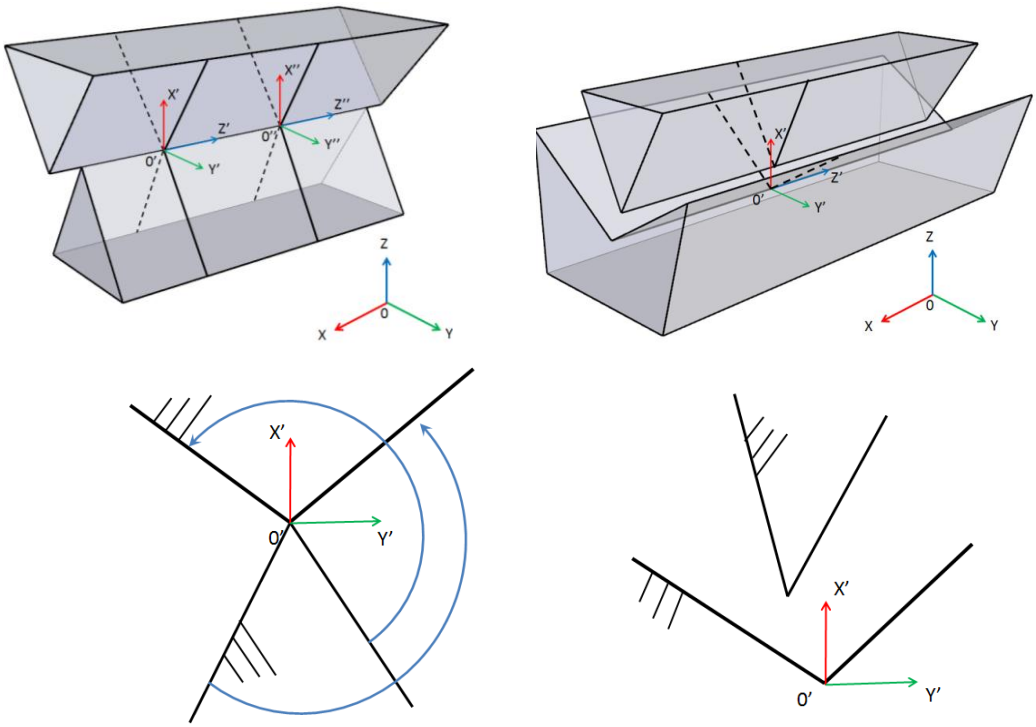

Figure 3- 7 Auxiliary section planes for 3-D parallel contact edges' type case

The situation that requires transforming is under the contact type of edge-to-edge (parallel), vertex-to-edge, and vertex-to-vertex. 1) *Edge-to-edge parallel:* Set up an auxiliary section plane along directional vector of edge, so that the 3-D contact type can be treated as a 2-D contact case, shown in Fig. 3-7. The contact between two 2-D angle has sufficient reference in (Shi, 1988). The entrance lines of 2-D contact algorithm should correspond to the entrance planes of 3-D contact cases. By this logic, this type of contact pair will be transformed to one or more pairs of first kind of entrance mode. Furthermore, each 3-Dparallel edges contact case should generate a pair of 2-D vertex-vertex contact models along the edge direction. 2) *Vertex-to-edge:* Setup an auxiliary plane to perpendicular to the average normal direction, so that vertex-to-edge is transformed to point-to-plane mode. 3) *Vertex to vertex:* the local section plane is setup and sampled 3-D vertex-to-vertex cases with 2-D slices, to help judgment. It is worth to notice that a vertex in such valley may have more than one contact pair involving. In other words, it has more than one entrance mode.

Step5: Judging Process

Judging process is to judge real contact pair under definition of entrance mode and penetration criteria. Entrance mode is to finally determine whether two contact pair candidates have met or not, and at the same time to guide the selection of the right location to add contact constraints to prevent the contact bodies from penetrating

each other.

Different from 2-D, contact judgment monitors the volume of the auxiliary tetrahedron. Indeed, we try to construct such auxiliary tetrahedron for both *mode 1* (Point-to-plane mode) and *mode 2* (Crossing-line mode) that a unified formula can be used to describe the relative position between the contact pairs. More specifically, as below: 1) Point-to-plane mode: There are two arbitrary shaped polyhedral elements coming into contact, as shown in Fig. 3-8. 2) Crossing-lines mode: When two edges belonging to different manifold elements approach close to each other until the happening of real contact, crossing-lines mode fits well. Similarly, we can construct an auxiliary tetrahedron as following steps, shown in Fig. 3-9. Then the contact situations for the contact pair candidate in different modes are determined and judged.

Step 6: Recording process

Recording process is to record contact pair information for next iteration step or time step. The recording information includes contact pair index, contact pair types, the number of entrance modes for current contact pair, open-closed state, penetration normal depth, relative tangential displacement, new contact identity.

After the contact checking procedure, penalty method is used for its numerical treatments of contact constraints in the current 3-D NMM, as it does not introduce additional new unknowns, although not the most accurate method. The 3-D normal contact matrix, tangential contact matrix and friction force matrix are derived (*refer to the thesis section 5.4)*.

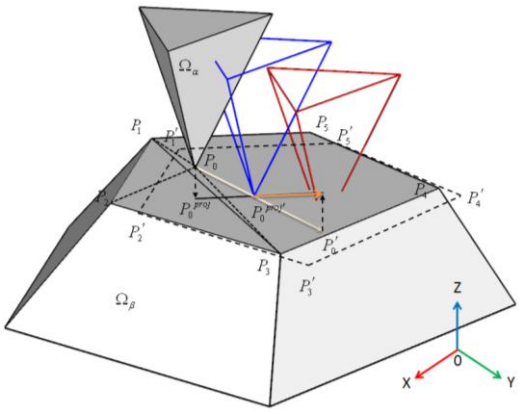

Figure 3- 8 Point to plane mode

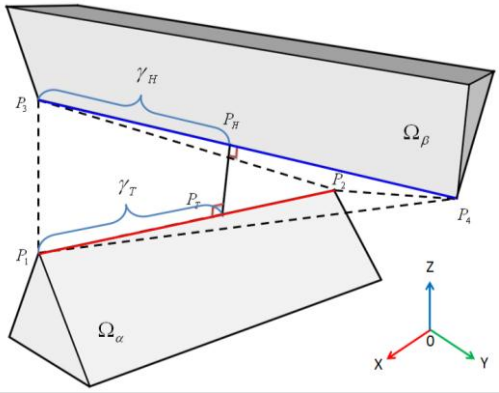

Figure 3- 9 Crossing-lines mode

Part 3-C: General Procedure in 3-D NMM Contact Program

The general incremental solution format with contact treatment capacity for 3-D NMM combines above-mentioned techniques to generalize solution procedure, including mechanics condition of contact interface, contact checking algorithm, the penalty way of introducing contact constraint into system functional based on generalized variational principle.

1) *Try and error iteration-------Open-closed iteration.*
The proposed 3-D NMM applies incremental formulation with implicit solution. In each time step, assembling and solving system of equations are repeated to determine correct contact pair position, and to apply contact springs to the right location. This trial-and-error iteration procedure is generally depicted as: a) Through contact checking algorithm (Step *1 2 3*), target potential contact pair candidates, say, there are number of ${}^{cpc}N$. According the result of the last time step (e.g., location of vertex, position of known contact pairs), the initial value of contact pair position and intensity are assumed for the first iteration step ${}^{try1}N <= {}^{cpc}N$. b) Based on the loading condition, recorded element information (e.g., element strain, velocity of vertex) in the prior time step, and initial guess value ${}^{try1}N$, the inequality constraints are overwritten to the equality constraints in kinematics and dynamics, which would be used as definite condition to reorganize the global systematic formula. c) Re-call the subroutine of contact checking algorithm, determine the real contact pair position under presumed guess value, denoting the number of real contact pair ${}^{res1}N$. Additionally, apply inequality constraints condition as verification condition. If the resulted ${}^{res1}N$ is consistent with the presumed ${}^{try1}N$ completely, also all ${}^{res1}N$ pairs satisfy the verification condition, the solution is done in this time step. Otherwise, return back to *step a)* to redefine the initial guess value and iteration solution until the verification condition bounds.

2) Verification conditions and corresponding operations on the contact interface
Besides the normal verification condition above, there are more strict contact interface verification conditions in 3-D NMM. The contact states on the interface have totally three kinds: stick, slide, and separate. Verification conditions are described to the three kinds consequently, shown in Table 3-1.

According to the verification condition, the following operations are listed below in Table 3-2:

Table 3- 1 Verification of contact situation in 3-D NMM

Contact State		Verification
Separate		$\left({}^{t+\Delta t}\boldsymbol{x}^{B} - {}^{t+\Delta t}\boldsymbol{x}^{A}\right)\cdot {}^{t+\Delta t}\boldsymbol{n}_3^{B} \geq \varepsilon_s$, If not, turn to "stick state"; record the position of contact
Contact	Stick	a) ${}^{t+\Delta t}\boldsymbol{P}_N^{A} = -{}^{t+\Delta t}\boldsymbol{P}_N^{B} \geq 0$, if not, turn to "separate state" b) $\left\|{}^{t+\Delta t}\boldsymbol{P}_T^{i}\right\| - \mu\cdot\left\|{}^{t+\Delta t}\boldsymbol{P}_N^{i}\right\| < 0 \quad (i = A, B)$, if not, turn to "slide state"
	Slide	a) ${}^{t+\Delta t}\boldsymbol{P}_N^{A} = -{}^{t+\Delta t}\boldsymbol{P}_N^{B} \geq 0$, if not, turn to "separate state" b) $({}^{t+\Delta t}\boldsymbol{u}_T^{A} - {}^{t+\Delta t}\boldsymbol{u}_T^{B})\cdot {}^{t+\Delta t}\boldsymbol{P}_T^{A} < 0$, $\left\|{}^{t+\Delta t}\boldsymbol{u}_T^{A} - {}^{t+\Delta t}\boldsymbol{u}_T^{B}\right\| < \varepsilon_s$, if not, turn to "stick state"

where ε_s is the numeral mite in contact checking procedure

Table 3- 2 Detailed operation corresponding to the change of contact state

State Changes	Corresponding Operation
Separate to separate	No change
Separate to slide	Apply the normal spring and a pair of friction force
Separate to stick	Apply the normal and tangential springs
Slide to separate	Release the normal spring and a pair of friction force
Slide to slide	No change
Slide to stick	Release the friction forces and apply the tangential spring
Stick to separate	Release the normal and tangential springs
Stick to slide	Release the tangential spring and apply a pair of friction force
Stick to stick	No change

3) The 3-D NMM codes flowchart (Fig.3-10)

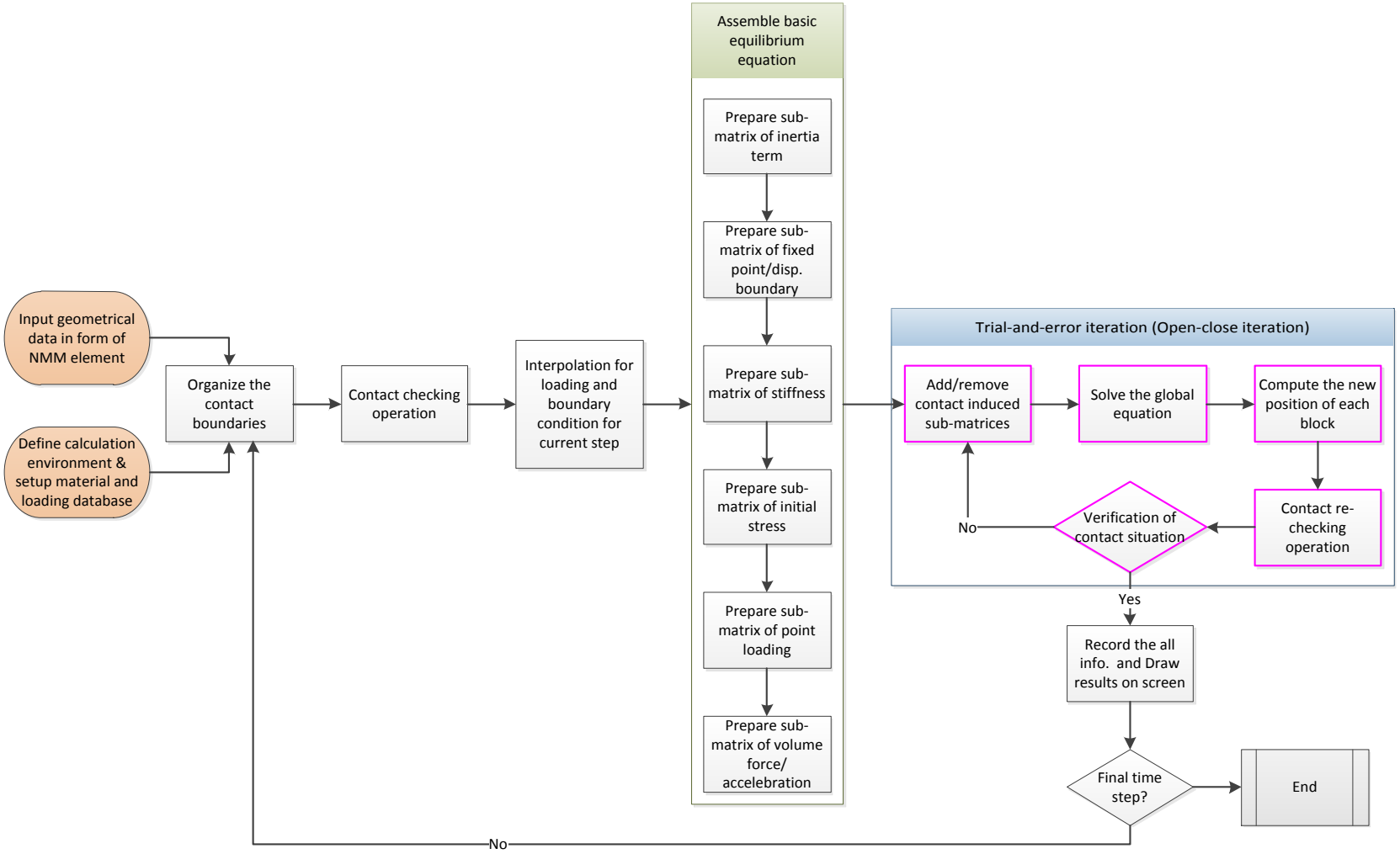

Figure 3- 10 Flowchart of 3-D NMM program with contact treatment function

Part 4: 3-D NMM Verification examples

In this part, the author is going to examine the precision and robustness of the 3-D NMM algorithm developed.

At first, the classic example of "*a free falling block*" is used to verify the predictability of the 3-D NMM to simulate the problem under continuous environment. Serial tests are followed by analyzing the "*effect of MC size*" and cutting plane "*orientations*" direction through a plane structure, which also verifies the convergence and stability of the continuum algorithm.

It then utilizes a case of "*a cube sliding on an inclined plane*" to examine the numerical contact algorithms (especially face-to-face, vertex-to-face), when imposing frictional boundary conditions.

Later, the precision of the 3-D NMM is examined by comparing with the analytical solutions from the parametric study on "*a roof wedge falling*" case.

In order to further demonstrate the function of 3-D analysis, a "*3-D tetrahedral wedge sliding*" case is designed and demonstrated the analytical ability of the algorithm. Finally, robust tests for multi-blocky system are undertaken by "*dominos run*" and "*dougong/bracket structure*" crushing are analyzed and discussed.

Verification Example: Free fall of a block

The free-falling process of a single block is simulated (shown in Fig. 4-1). The cube falls under the only influence of the gravity (10 m/s^2). The adaptive time step is initiated at 0.05s. The displacement and the velocity time history are shown in Fig. 4-2. The dots are the results of 3-D NMM simulation, while the curved lines as exact value from the analytical solution. The error between them in the maximum absolute difference is less than 0.1%, which illustrates the credibility of the NMM calculation.

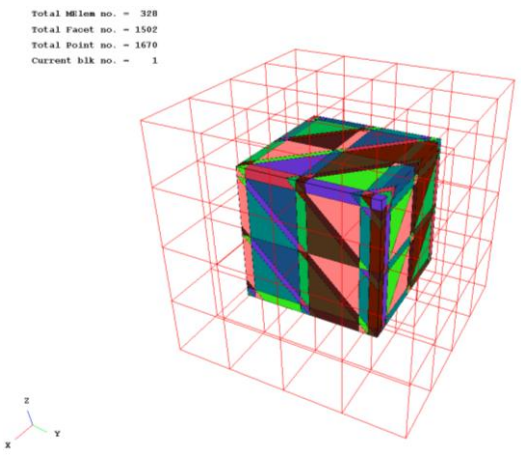

Figure 4- 1 Falling cube under gravity

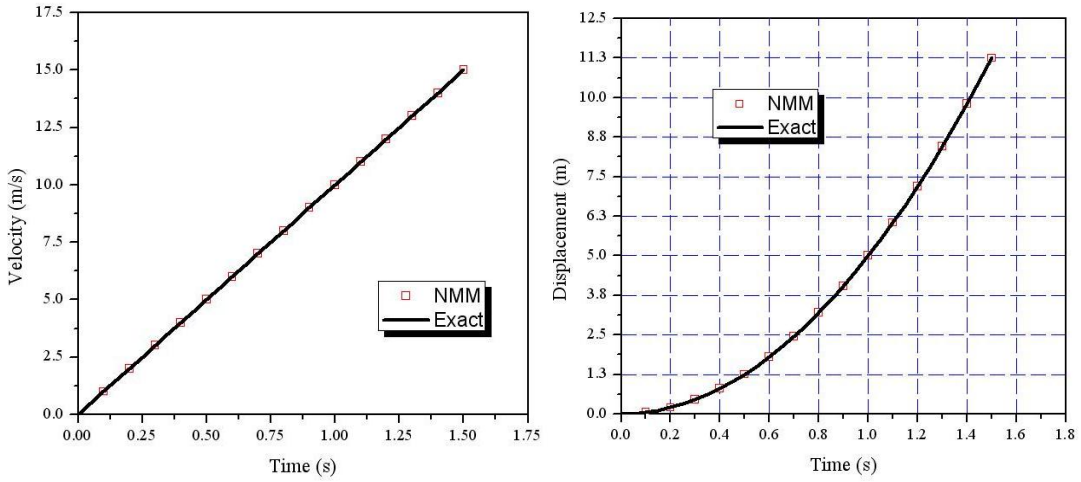

(a) Velocity history (b) Displacement history

Figure 4- 2 NMM and analytical results on displacement & velocity history

Verification Example: Effect of MC Size and Orientation

The following examples are to investigate the effect of the manifold cove (MC) size and the cutting plane orientations. In a quasi-static condition, a 2 m×2 m×0.1 m plate is subjected to the gravity load (10m/s^2) and fixed at four corners. The material properties are set as *E=10kPa, v=0.3, m=12* kg/m^3. Its geometry of the typical mesh design is shown in Fig. 4-3 in which the faces of the plate are conformed parallel to the axis planes.

Six mathematical cover size of s= 0.52, 0.32 0.22, 0.12, 0.08 and 0.05 are used, and 190, 684, 1104, 3706, 8100 and 19200 manifold elements are respectively generated after intersecting with the physical plate. Five measurement points are set to clarify

the quasi-static responses (Fig. 4-3). The calculated results are converging and stable with the increase of the mesh density (Fig. 4-4) and the analysis are listed in Table 4-1.

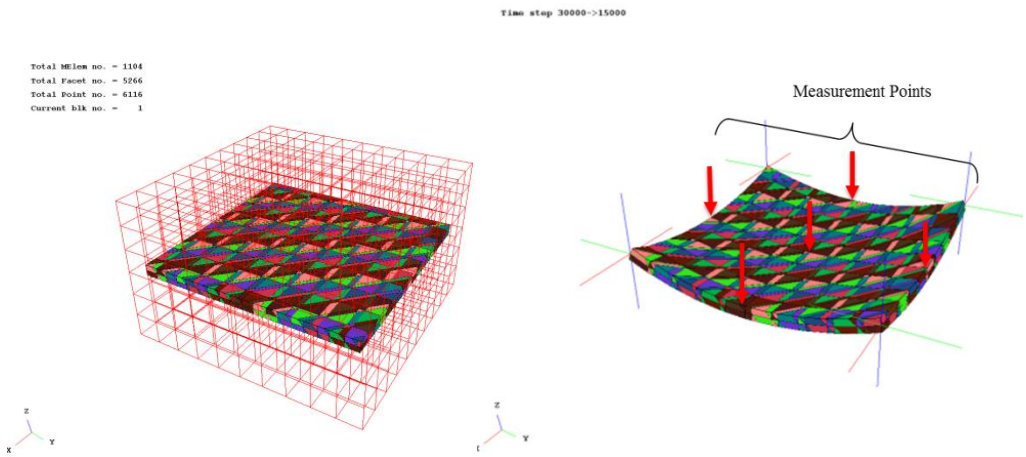

(a) Mesh design #1 (b) Location of measurement points

Figure 4- 3 Geometry of typical mesh design for *mesh density effect study*

The maximum displacement of case 6 (*refinement 5*) is illustrated in Fig. 4-4. Results converge well and all four edges are adequately symmetric, e.g. M1~4 curves in Fig. 4-4 represent the deformation history of four middle points from the up, down, left and right side. The results converge to the closed-form solution when the mesh density increases. The validity of the 3-D NMM calculation is supported by the consistent results given by the FEM analysis solution.

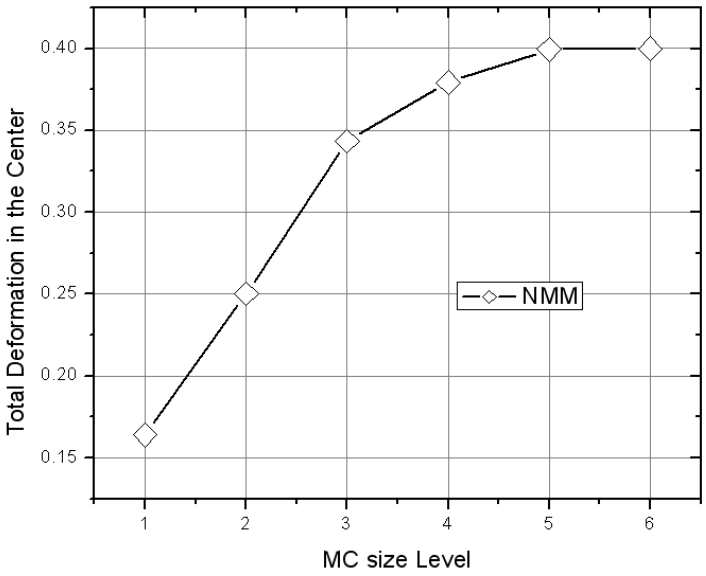

Figure 4- 4 Total deformation convergence test

Table 4- 1 Solution history at the center of panel

Name	Base Solution	Refinement 1	Refinement 2	Refinement 3	Refinement 4	Refinement 5
Total Deformation	0.16404 m	0.25027 m [+34.45%]	0.34334 m [+27.11%]	0.37919 m [+9.45%]	0.39694 m [+4.47%]	0.39973 m [+0.76%]
Mesh properties	**Spacing**					
	0.52	0.32	0.22	0.12	0.08	0.05
	Elements					
	190	684	1104	3706	8100	19200
	Vertexes					
	1156	3812	6116	20184	44282	76800

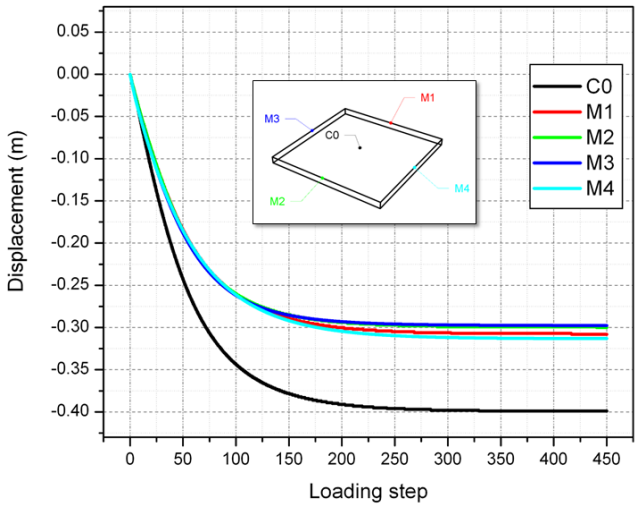

Figure 4- 5 Deformation of case 6 at the maximum displacement loading step

In dynamic condition, the MC orientation effect is tested by *the same* size plate, with a constant point load *L=5 kN* at the center with four fixed corners. Two different orientations of the mathematical mesh (Orientation *2 and 3*) are shown in Fig. 4-6 while the orientation 1 is same as *above*.

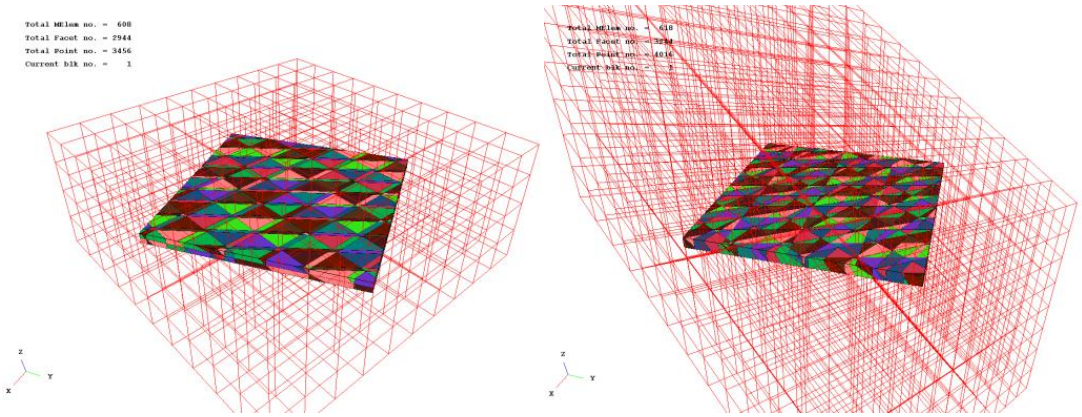

(a) Mesh design #2 (b) Mesh design #3

Figure 4- 6 Geometry of mesh designs for *mesh orientation effect study*

The *Z* displacement histories of the center point are shown in Fig. 4-7, where the orientation of the MCs has negligible effect on the plate maximum displacement at the plate center. The maximum displacement is accurate and stable after converging, and the convergence time is similar when the total element number is almost same. The details of results could be found in the thesis.

It shows that the orientation of the MCs has little effect to the simulation result. This ensures the accuracy and modeling efficiency of the 3-D NMM decreasing the mesh division complexity in FEM.

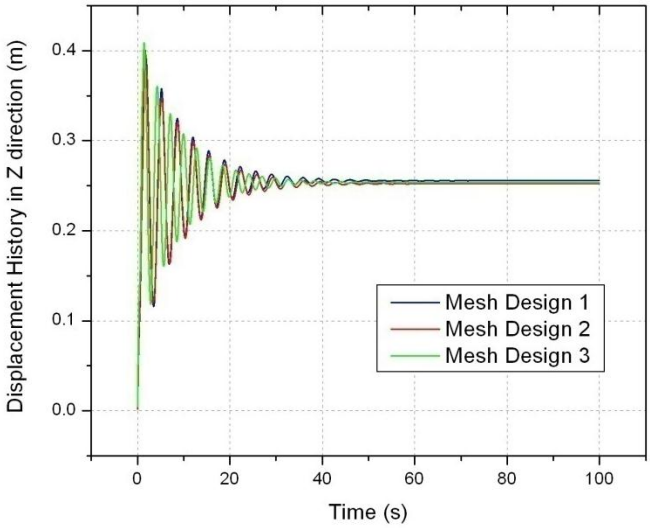

Figure 4- 7 *Z* displacement histories of center point

Verification Example: Cube Sliding on an Inclined Plane

This example is designed to test the numerical algorithms in the face-to-face contact mode (or vertex-to-face mode), and the stability of the system in applying friction boundary condition.

A matrix sliding cube is put on an inclined plane, and the movement of the sliding cube is observed. The general equation of motion for a rigid block on an inclined plane subject to *Coulomb* frictional resistance force can be expressed as a single degree-of-freedom system by taking its coordinate system parallel to the plane direction, as shown in Fig. 4-8 (1). The analytical solution for the displacement *d* after time *t* from the resting state is:

$$d = \frac{1}{2} g \left(\sin \alpha - \tan \phi \cos \alpha \right) t^2 \qquad (4\text{-}1)$$

where g is the acceleration of gravity, α is the slope angle of inclined plane, and ϕ is the friction angle of plane surface.

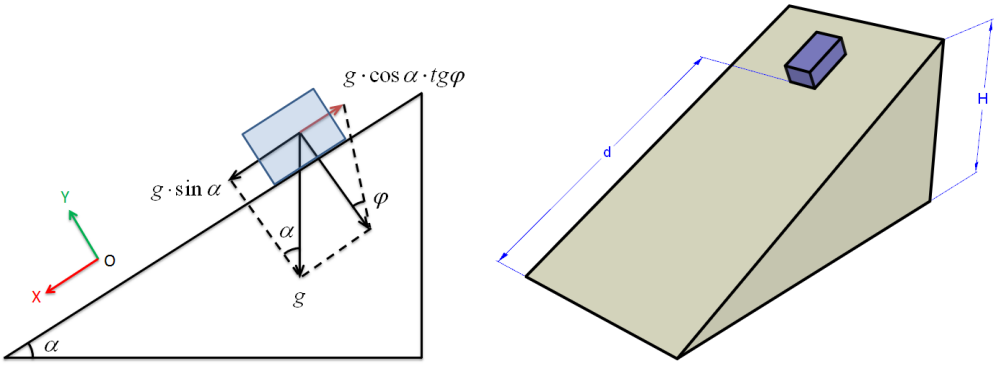

(1)General model (2) Physical model

Figure 4- 8 Sliding Cube on an Inclined Plane

The physical model consists of two contact bodies (Fig. 4-8 (2)). The bottom wedge with inclined plane is fixed and only the sliding cube is allowed to move under the pure gravity (*Detailed parameters could be referred in the thesis*).

After the intersection between the physical model and mathematical covers, 280 tetrahedron manifold elements are finally generated (Fig. 4-9). Seven different friction angle values, with 0, 5, 10, 15, 20, 24, 25, have been assigned on the sliding surface.

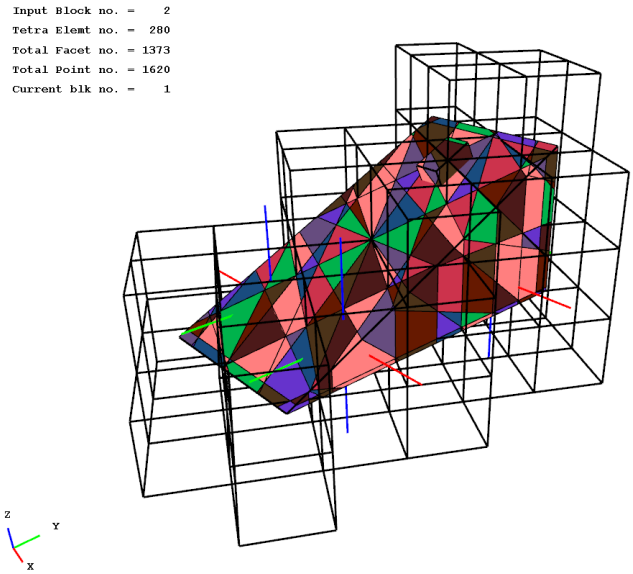

Figure 4- 9 Tetrahedron manifold elements for calculation in "Cube sliding"

A comparison between the analytical (Eq. (4-1)) and 3-D NMM solutions is shown in Fig. 4-10. 3-D NMM results show a satisfactory agreement with the time-dependent

displacement functions predicted by the analytical solutions, where the maximum error is less than 0.001% for all different friction angles tested.

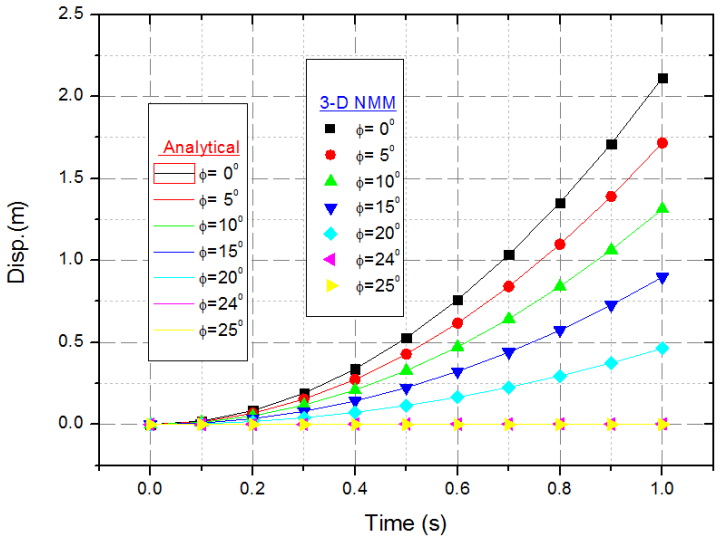

Figure 4- 10 Comparison between the analytical and 3-D NMM results in "Cube sliding"

Verification Example: Roof Wedge Falling

The stability of a rock mass located at the roof of a tunnel is always the priority concern. The stabilizing effect of the in-situ stresses and the influence of joint friction are significant factors that affect the structure stability of tunnels. Under the effect of these two factors, tunnel surface could stay stable without any artificial supports. Meanwhile, sudden change of the intensely strong in-situ state of stress and joint friction state could be one of the reasons to induce rock burst. A simple model in this example is first used to examine the accuracy of the 3D-NMM analysis prior utilizing it to analyze the stability of the complex tunnel structure.

Fortunately, the simplified model of falling wedge has a theoretical solution. A closed-form solution of the support force for stabilization of the wedge in the roof was derived by (Goodman et al., 1982) (*Details could refer to thesis*). For this particular case, where: 1) All joints have the same dip angle; 2)The initial stress state in the plane parallel to free face of the block is hydrostatic; 3) All joints have the same ratio between normal and shear stiffness.

The critical friction coefficient required for stability of the wedge without any support can be expressed by Eq. (4-2):

$$\tan\phi = \frac{W + \sigma_n \sum A_i \sin\alpha}{\sigma_n \sum A_i \sin\alpha - W \tan\alpha} \tag{4-2}$$

where

n = number of faces on the block; i = index denoting the face of the block;

A_0 = required force to stabilize the wedge; W = weight of the wedge;

$\sigma_{n,i}$ = normal stress acting on the i^{th} face of the wedge;

A_i = area of the face of wedge; ϕ_i = friction angle on the face of the wedge;

α_i = complement of the dip angle of the joint which creates the face;

The hexahedron manifold elements with corresponding mathematical covers are presented in Fig. 4-11.

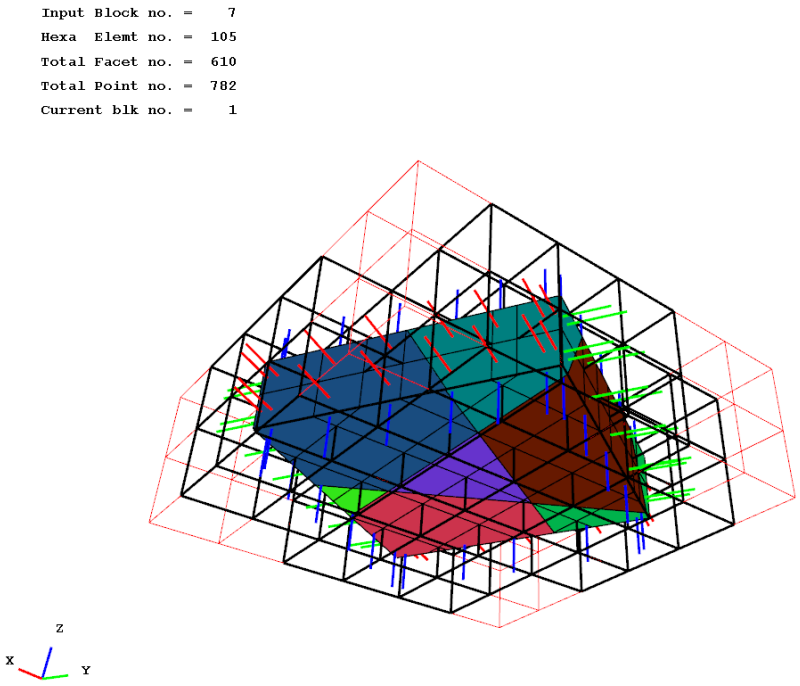

Figure 4- 11 Hexahedron manifold elements with mathematical domain

After intersection between the physical model and mathematical covers, 454 manifold elements are finally generated. The 3-D NMM simulation yields a friction angle 36.354^0, and the closed value from the analytic solution for the critical friction angle is 34.402^0. The failure process of the wedge is simulated (Fig. 4-12).

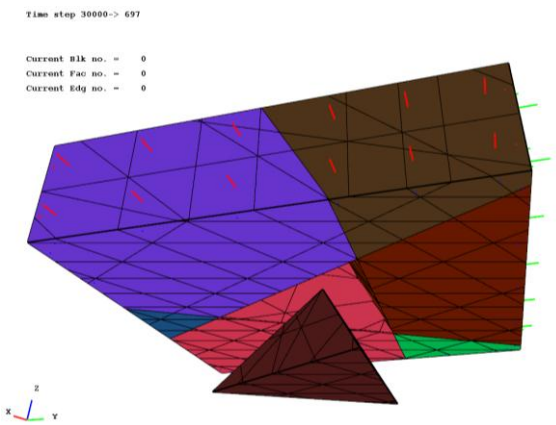

Figure 4- 12 Failure of roof wedge

Although, the final result of this example has an error of 5.67% compared to the analytical solution, it illustrates the reliability of the contact algorithm & its initial strain imposed and also proves that the calculation precision of 3-D NMM has satisfied the practical rock engineering requirements.

Verification Example: Tetrahedral Wedge sliding

Rock-slope failure is a major hazard in cutting highways and railways in mountainous area. A tetrahedral wedges sliding is one of most common phenomena. A tetrahedral wedge is designed (Fig. 4-13). One vectorial procedure in previous study is chosen to check the analytical ability of 3-D NMM to this kind of problem (*Detailed description and equations refer to the thesis*).

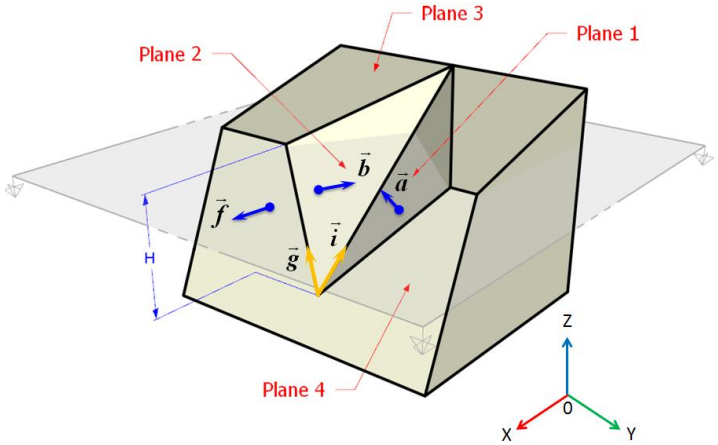

Figure 4- 13 Definition of the slope geometry

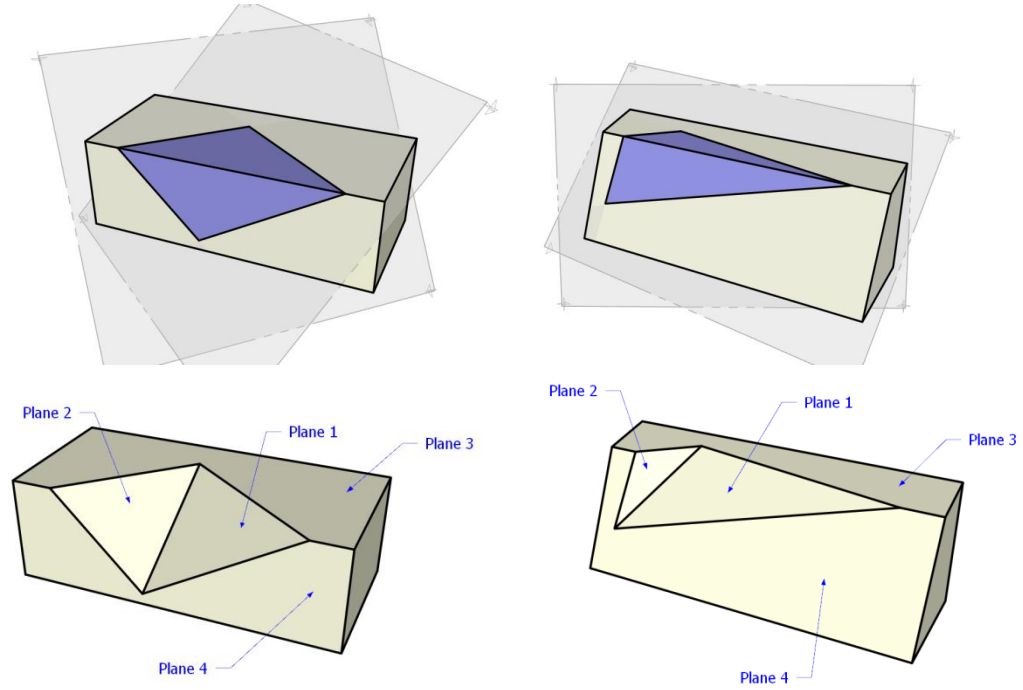

Case (a) Case (b)

Figure 4- 14 Physical models for sliding wedge

It examines whether the failure mode could perform as expected by sliding through the specific planes (Fig. 4-14 and Fig. 4-21). 4 planes' Dip and DD, with stereographic projection are shown in Fig. 4-15.

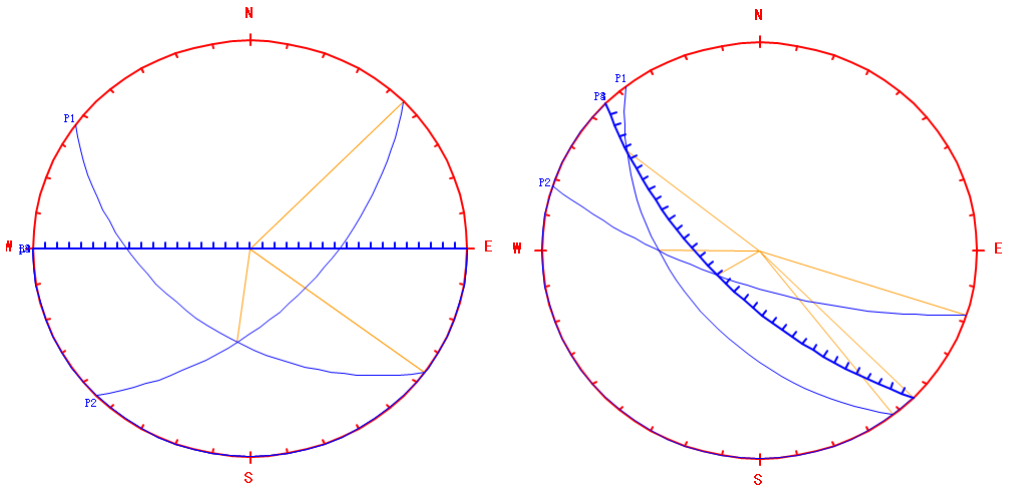

Figure 4- 15 4 planes' Dip and DD, with stereographic projection

For case (a), the calculation involves 292 manifold elements with mesh size 0.5 and Case (b) has totally 752 manifold elements with mesh size 0.5.

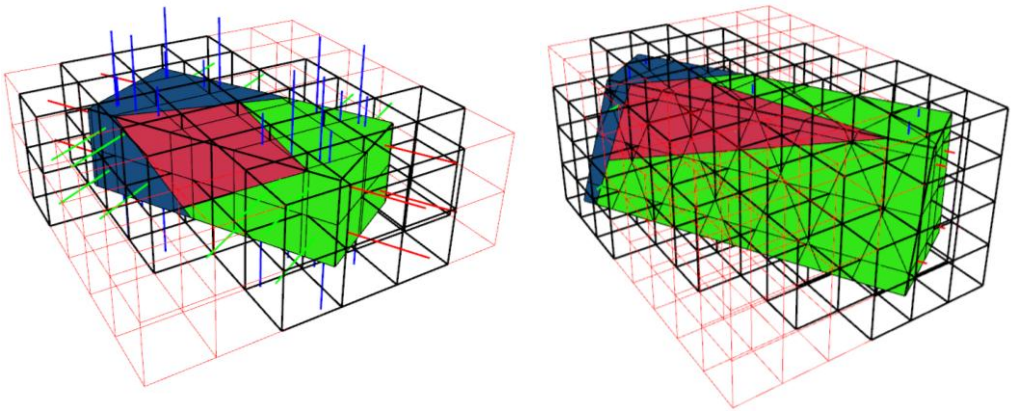

(a) (b)

Figure 4- 16 Hexahedron manifold elements with mathematical domain

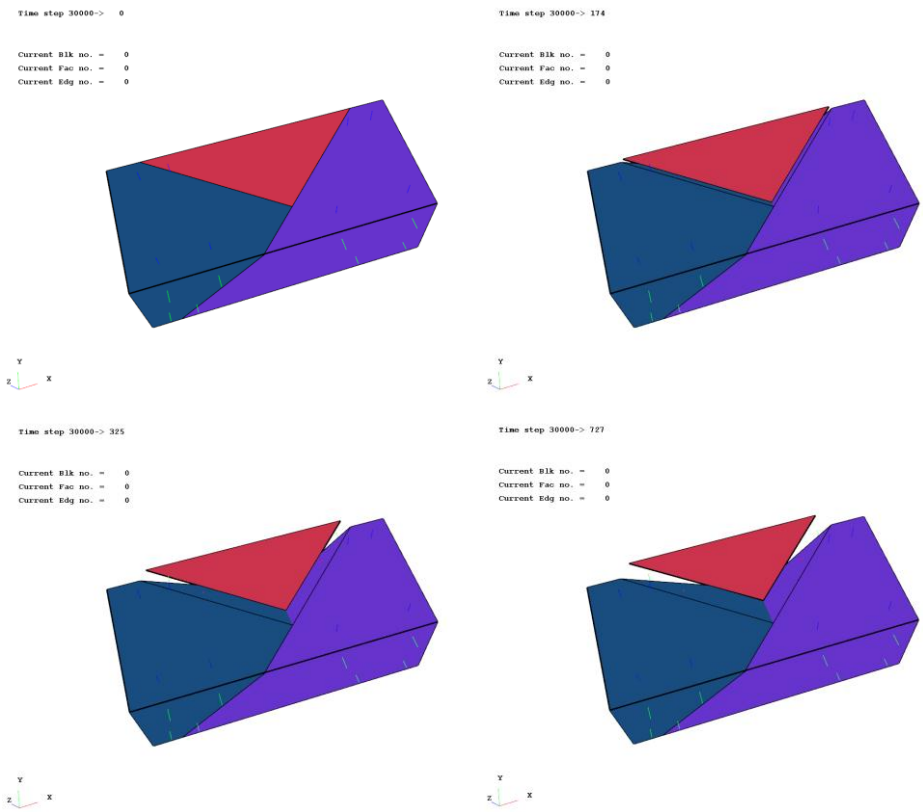

Case (a)

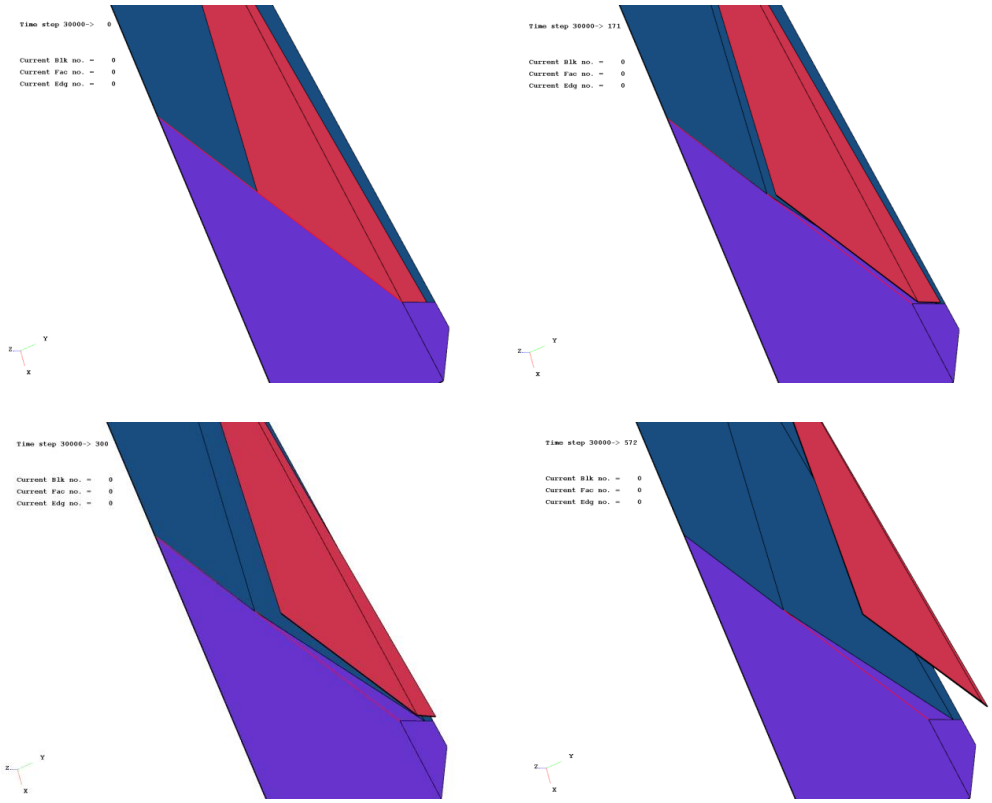

Case (b)

Figure 4- 17 Failure procedures according the predicted mode

The sliding situations in the numerical process are in line with the analytical prediction, as shown in Fig. 4-17.

Verification Example: Dominos Run

In order to test the ability to solve some discontinuous analysis problem, application problems such as dominos run and dougong/bracket structure crushing are analyzed and discussed. A typical 3-D domino run problem (Fig. 4-18) is numerically investigated using 3-D NMM. Different situations are studied. For example, the two-side simultaneous domino motion is shown to stop at the time of 2.05 second, where the ninth block and the tenth block will lean against each other as " Λ " shaped.

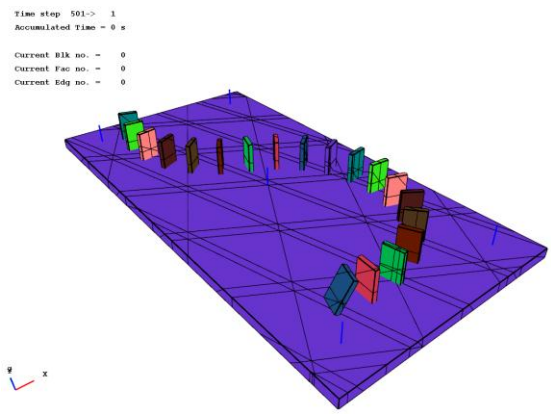

(a)0s

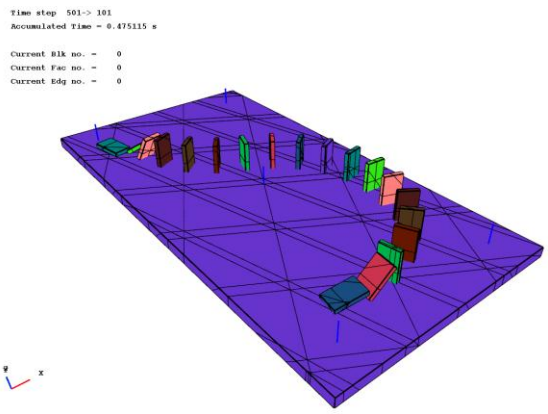

(b)0.475s

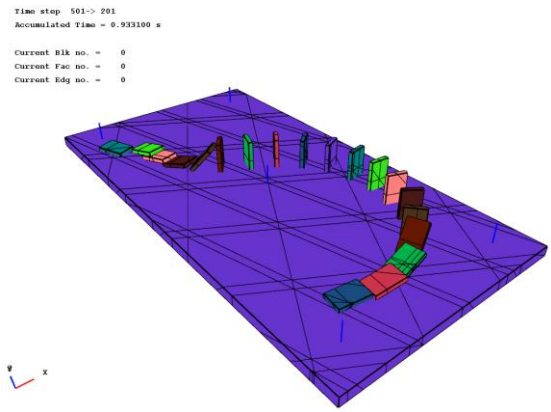

(c)0.933s

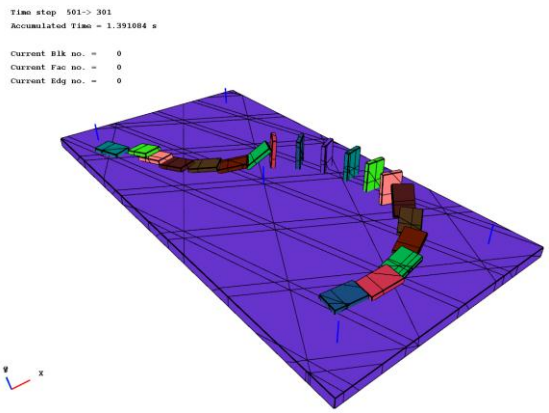

(d)1.391s

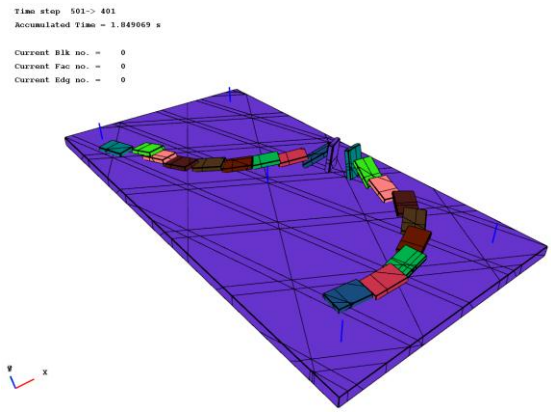

(e)1.849s

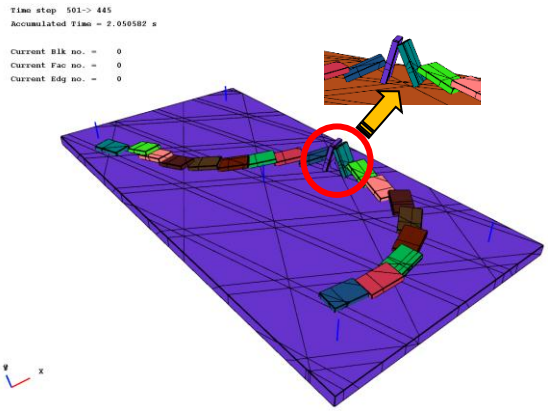

(f)2.051s

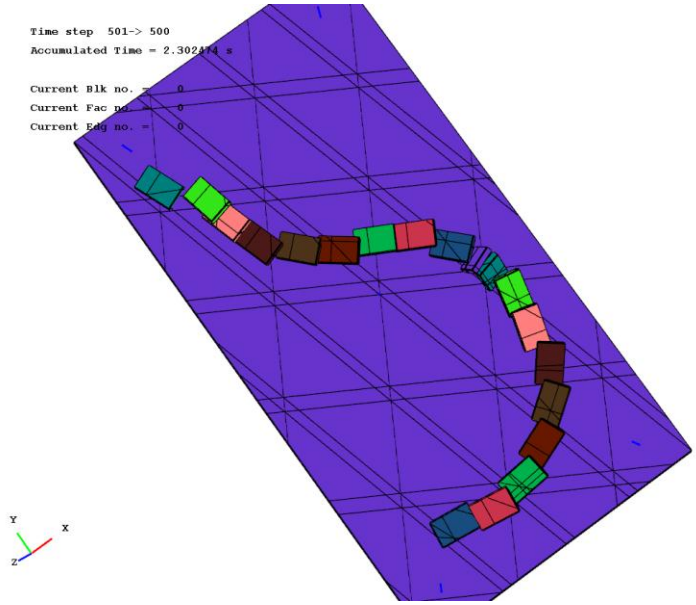

(g) Top view of dominos run at 2.302s

Figure 4- 18 Two-end dominos run process modeled by the 3-D NMM

Verification Example: Dougong/Brackets Structure

To test the ability of the proposed 3-D NMM to solve discontinuous problem, especially the consistency of crossing lines mode in the 3-D contact algorithm. A simplified dougong structure sample (Fig.4-19), which is subjected to pre-damage and lack of stability, is studied in 3-D NMM. The *dougong* style (also known as corbel arch, and Tou-Kung) wooden brackets structure, is built up from fixed layers of crossbeam fixed on top of columns, which is used in the design of *China Pavilion* in *World Expo 2010*, Shanghai (*Detailed description for the structure refers to the thesis*).

Such positioning makes the contact type to be mainly *crossing lines mode*, caused by face-to-face contact. The key problem that we concerned is "Whether the whole process of crashing-down damage satisfy the non-penetration contact condition?". If it always satisfies the non-penetration contact condition in the whole process, it will provide a strong support on the ability of 3-D NMM to solve similar contacting problems. The physical model interacts with the mathematical background, which generates numerical calculation mesh with 326 manifold elements, and detailed calculation description could be referred to the thesis.

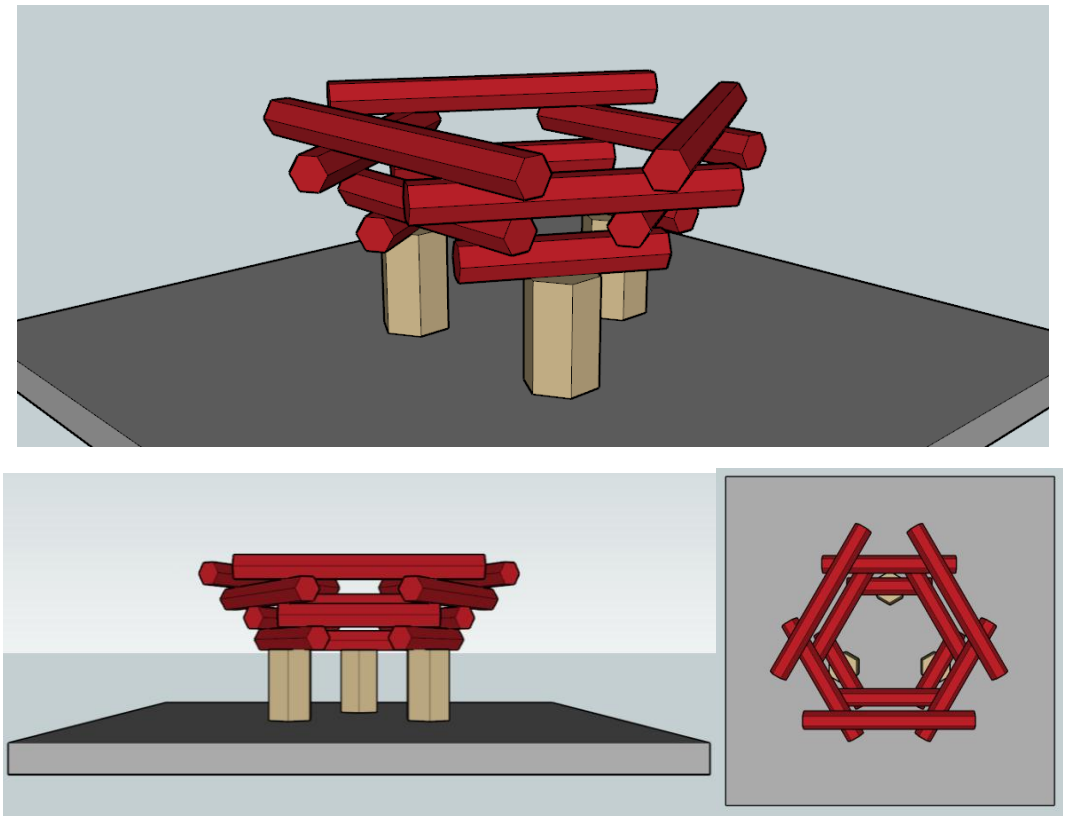

Figure 4- 19 Design of “dougong” structure model

For numerical simulation, one of the poles has been imposed by thorough-crack with a dip of 27.2 degree, which is the only one fault in the designed dougong structure. Under this case, the structure could be crashed down by the force of gravity and insufficient frictional resistance. Some configurations of the structure are shown in Fig. 4-20. It is proven to be efficient algorithm with its strong power of the implemented contact algorithm.

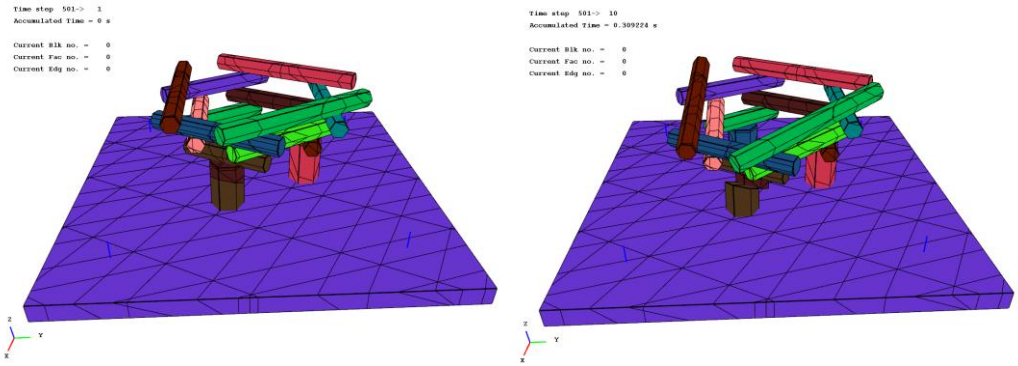

(a) 0s (b) 0.309s

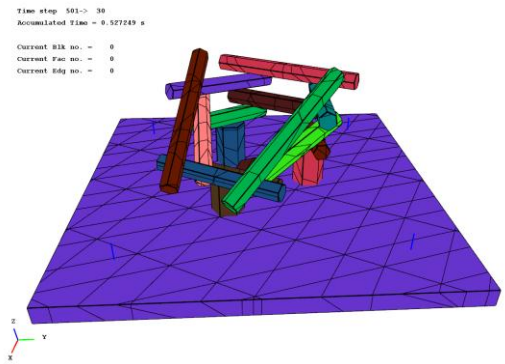

(c) 0.527s

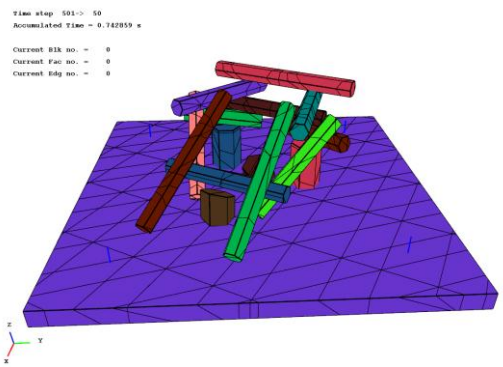

(d) 0.743s

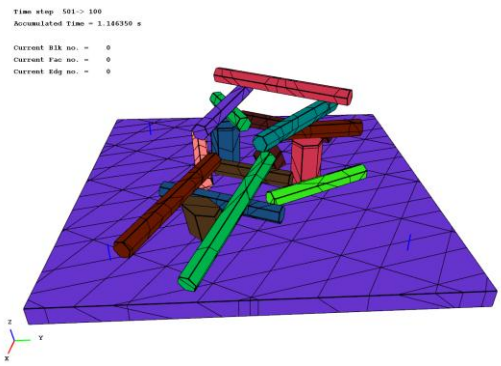

(e) 1.146s

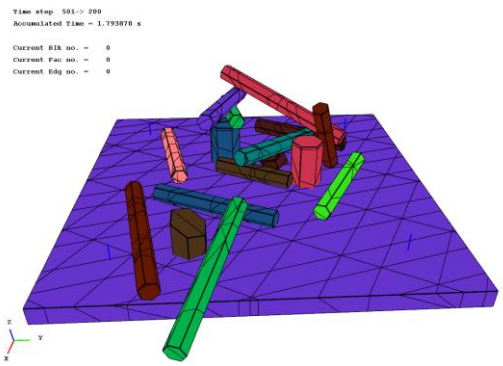

(f) 1.794s

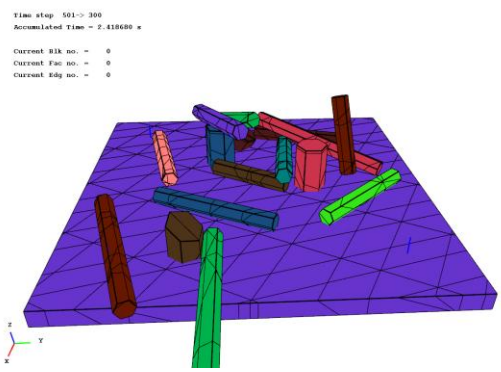

(g) 2.419s

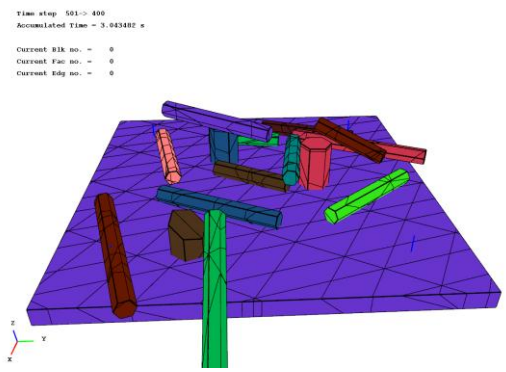

(h) 3.043s

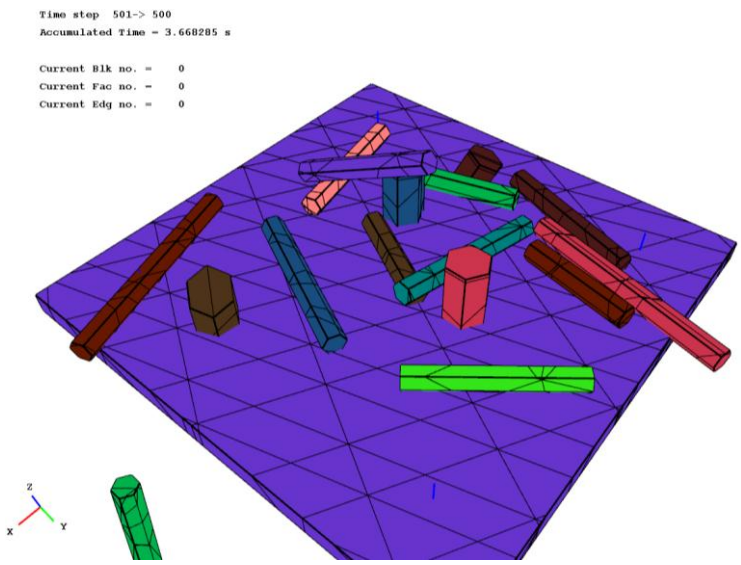

(i) 3.668s

Figure 4- 20 Failure process of "dougong" sample modeled by the 3-D NMM

Part 5: Engineering Applications

Engineering Application: Rock slope Stability Analysis

A rock slope scenario near an express-way is designed, as shown in Fig. 5-1. Specific description on its geometric modeling could be referred to the thesis. The main set of joints is almost parallel to the slope surface. Their dips get close to the initial natural friction angle of joints. It may cause the sliding of isolated blocks. As no crack propagation mechanism in current program, the model is discretized into 45 rock blocks that are likely to move out. The average volume of the rock blocks is 1.22995 m^3. The smallest block is 0.4155m^3, and the largest block is 2.7687m^3.

Based on 130 DST tests (Barton, 2008), the residual friction angle for rock joints is around 26^o~29^o with the roughness profile (JRC) and joint wall strength(JCS) description. Accordingly, a typical rock joints properties are assigned to this scenario example, and other parameters that used in 3-D NMM are also listed (in Table 5-1).

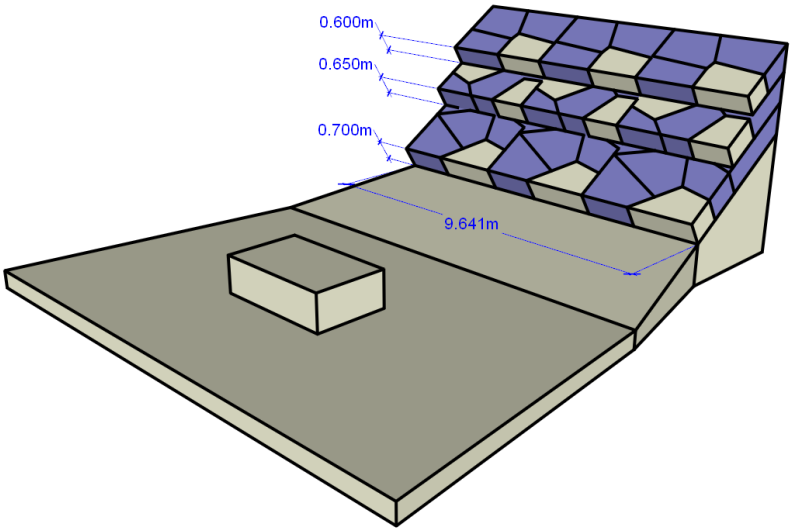

(a) ISO review of rock slope example

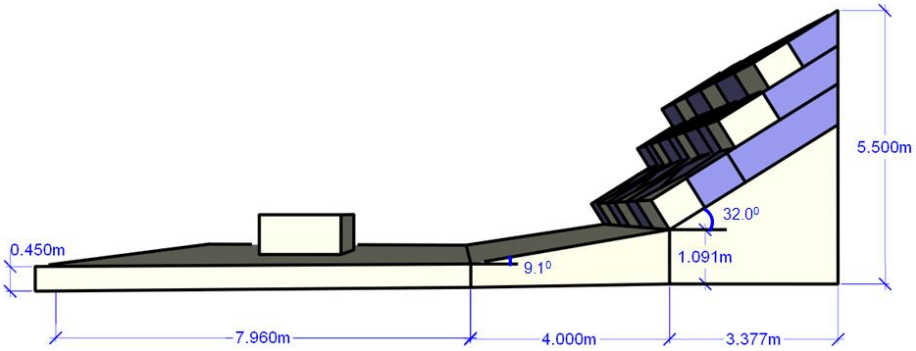

(b) Side view

Figure 5- 1 Configuration of designed rock slope example

Table 5- 1 Parameters in "Rock slope" example

Feature	Item tested	Value
Rock mass	Unit weight (kN/m^3)	25.7
	Poisson's ratio	0.23
	Young's modulus (GPa)	24.5
Discontinuity	Initial frictional angle (ϕ)	26.4
	Cohesion (MPa)	0.0
	Tensile strength (MPa)	0.0
Analysis parameters	Displacement-allowed ratio	0.01
	Maximum time increment (s)	0.001
	Normal contact spring stiffness (MN/m)	260.0
	Total time steps	10000.0

After the 3-D NMM preprocess treatment, the intersection between the physical model and mathematical covers, 1067 tetrahedron manifold elements are finally generated for the case.

Case A: Free sliding without lateral constraints

Assuming that only slope bottom, transition zone, and highway are fixed in this example, the 45 isolated blocks in the slope will slide down freely without lateral confinement pressure, where the friction angle has been set to 10^{o}. As the friction angle is smaller than slope grading angle, the blocks in the slope will not stay stable under the force of gravity. Fig. 5-2 shows the whole collapse of the slope in a large scale. In order to clearly analyze detailed slope sliding during the process, 9 representative blocks are chosen to depict the displacements from the 45 potential slide blocks, as in shown Fig. 5-3.

In Fig. 5-3, "B8" means the #8th block in this horizontal Group. "L1" means the #1st layer. "G1" indicts the #1st group in horizontal direction. The displacement curves of the selected 9 block's centroid are depicted, in Fig. 5-4.

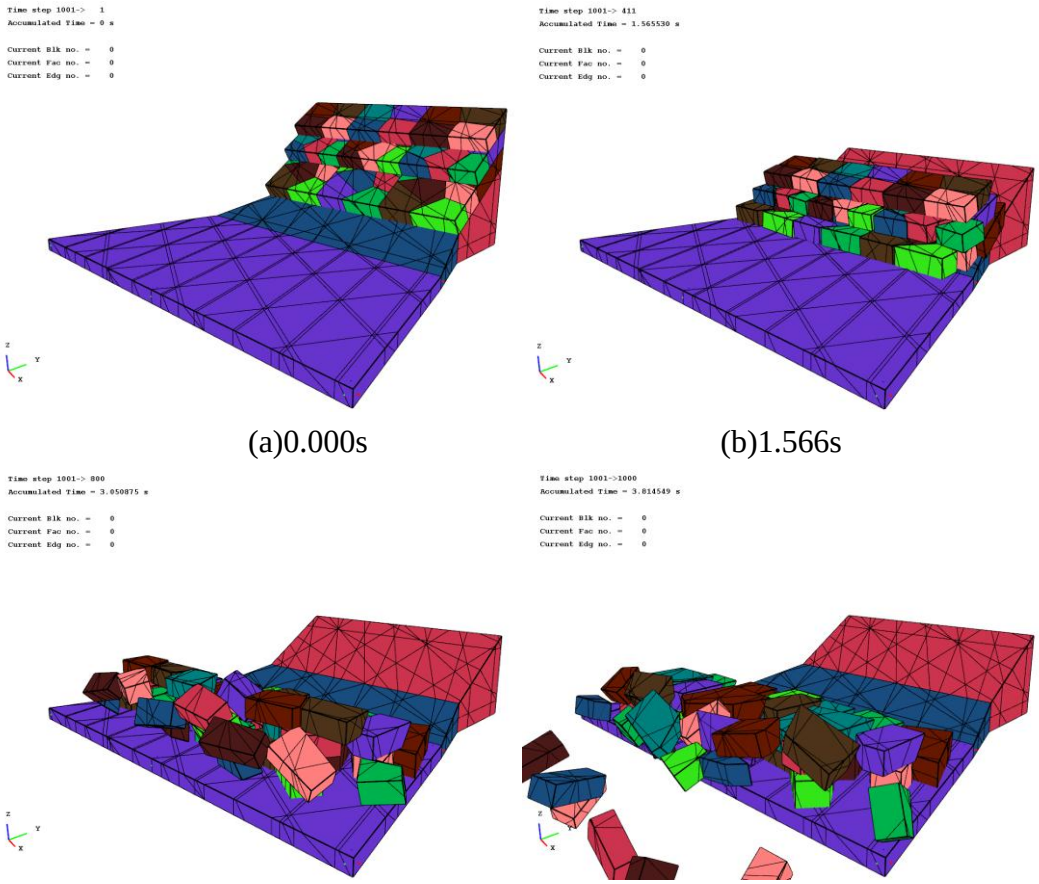

(a)0.000s (b)1.566s

(c)3.051s (d)3.815s

Figure 5- 2 Rock slope failure process modeled by 3-D NMM

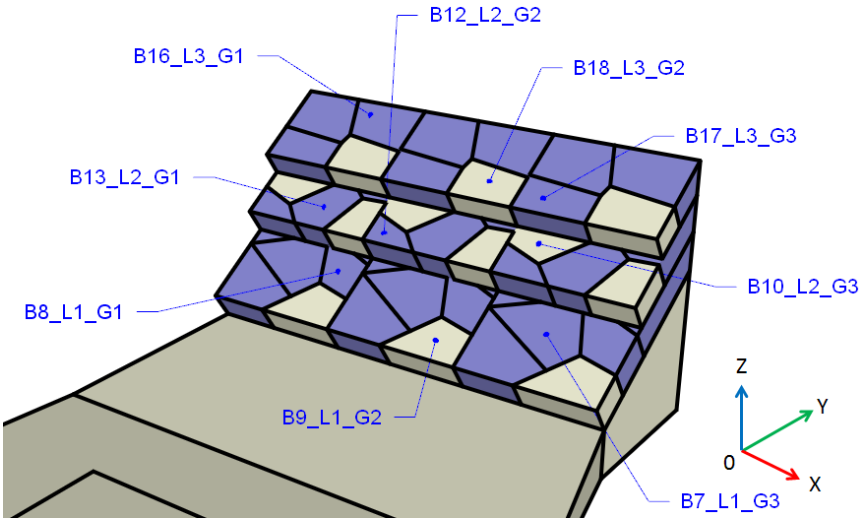

Figure 5- 3 Selected measuring blocks in "Rock slope" example

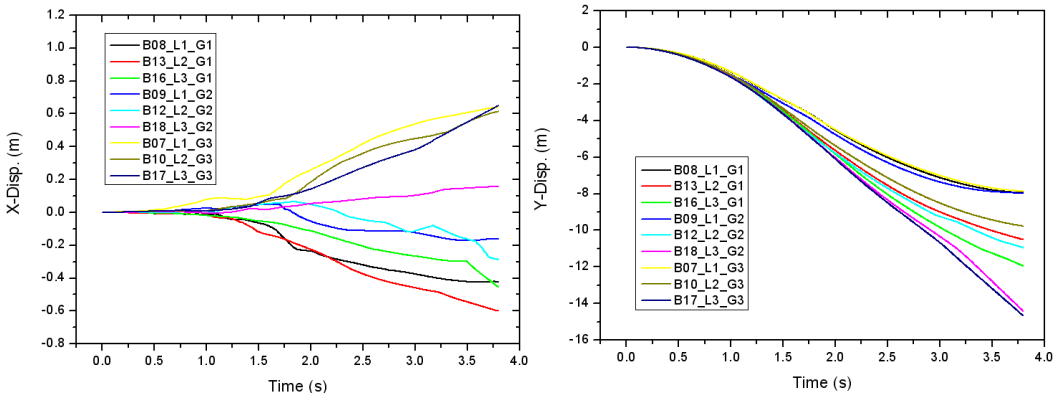

(a) Displacement history in X direction (b) Displacement history in Y direction

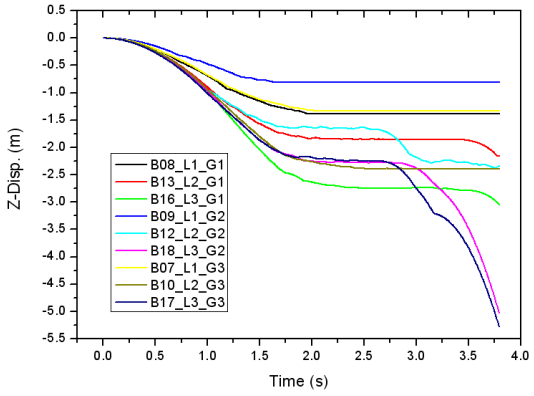

(c) Displacement history in Z direction

Figure 5- 4 Displacement history for selected blocks

The numerical results based on the algorithm has a great potential to provide more detailed information than traditional experiments, such as the detailed movement displacement curves. This information is a key and essential to design proper buttress and protection solution. At the same time, it also acts as important prerequisite to the inverse problem analysis.

Case D: Stabilisation technique- Fences barriers

Despite the above method of buttress, practical engineering also use barriers of fences to protect the highway to be damaged or to reduce its damage (as in Fig. 5-9) frequently. The method of fence does not prevent falling down of blocks; instead it reduces the damage degree. In practice, there might be wire netting between the bollards to prevent spillage of small relics during the slopes sliding. The current 3-D NMM has not yet included mathematical line model, hence the part of wire netting is neglected up until now.

A group of concrete columns (bollards) with a width of 450 mm and a height of 1700 mm are set at the transition zone between the highway and the potential failure slope. Assuming the bollards are sturdy enough, the simulation result is shown in Fig. 5-10. The total lasting time of calculation takes 9.0 s, the effect of the bollards is acceptable. Except some of small volume blocks falls outside to the road, most of falling blocks are fended within the transition zone.

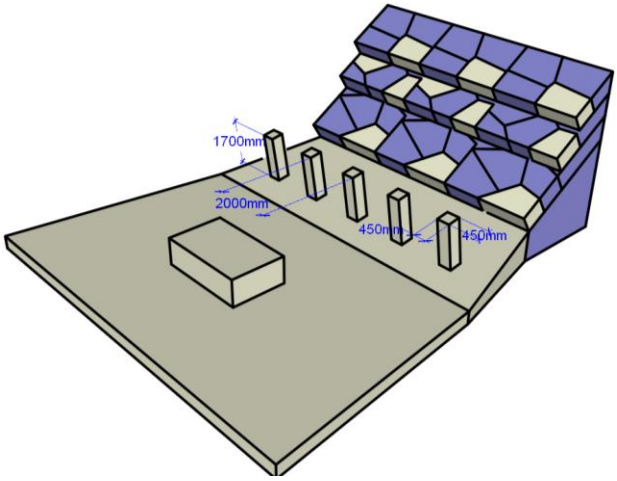

Figure 5- 5 Configuration of road barriers

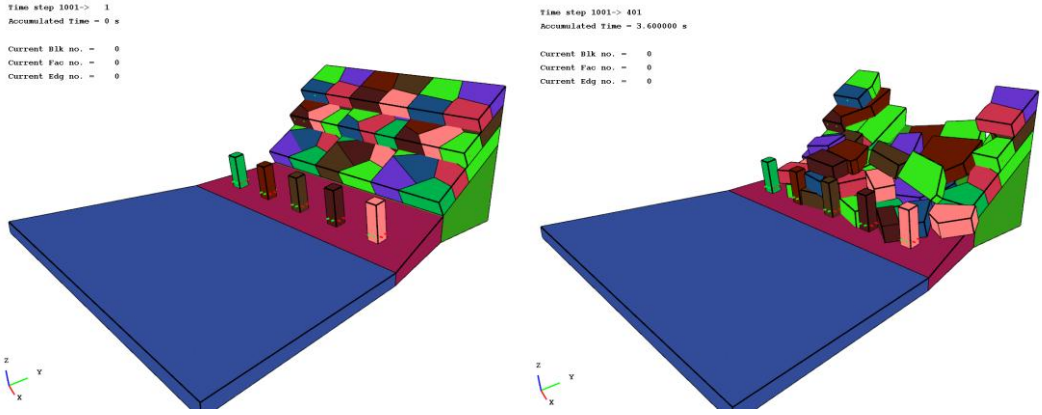

(a) 0.000s (e) 3.600s

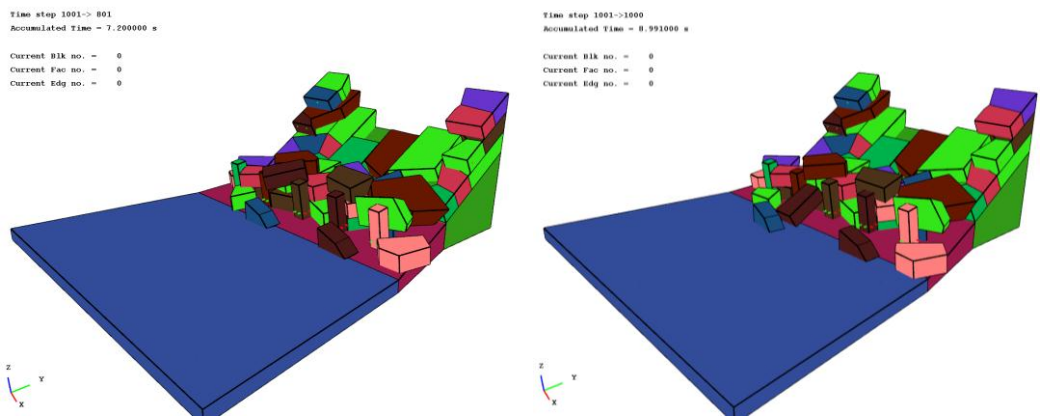

(i) 7.200s (k) 8.991s

Figure 5- 6 Road protection from rock slope failure by barriers

This engineering application presents a detailed implementation applied to analyze the failure process of a rock slope. The comparison between Case A and Case B shows the significant role of correctly determining in-situ condition for the rock slopes. Meanwhile, the ability of the developed 3-D NMM procedure to model a fairly complex failure process of a rock slope also highlights the inadequacy of a 2D analysis often used in practice.

Engineering Application: Rock Tunnel Stability Analysis

This part undergoes the dynamic analysis on complete failure process for key blocks in tunnel with 3-D NMM. By this way, some regular failure patterns are also recognized, which provides better references to practical rock engineering. Rock falling from the side and roof of tunnel surface is one kind of frequently seen accident during the excavation operation. Such falling blocks are the key blocks. Due to the loss of key block, more free-surfaces are exposed, which would produce more massive collapse. Therefore, it is an important task to find and describe the most critical key block around an excavation in such engineering problem.

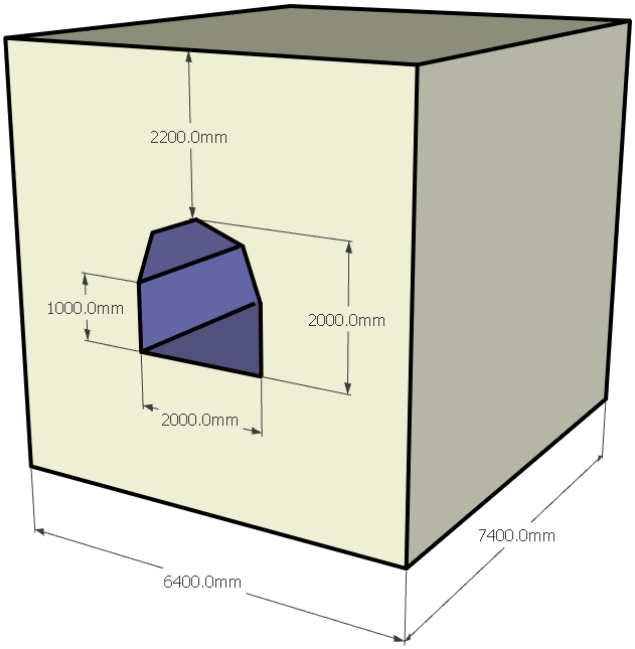

(a) Perspective view

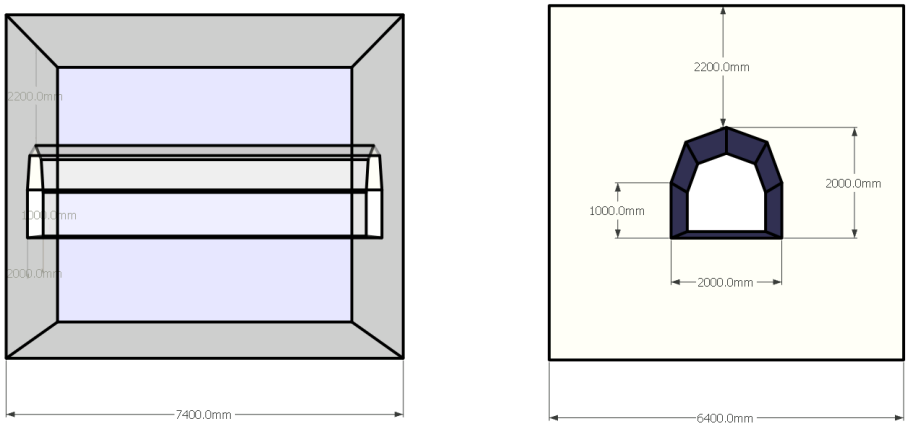

(b) Side view and front view

Figure 5- 7 Scenario setting for a rock tunnel

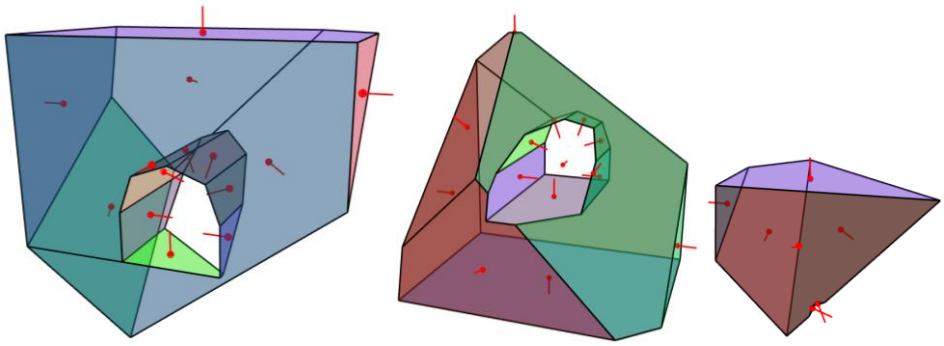

#01(63.4423 m^3) #02(86.9571 m^3) #03(11.2796 m^3)

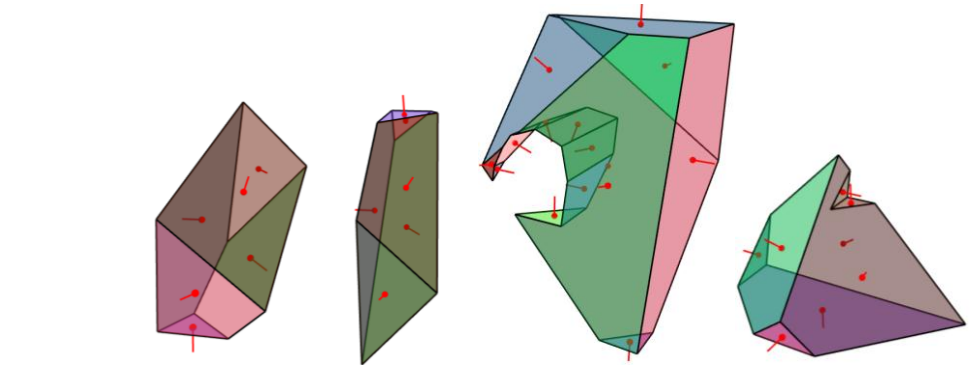

#04(9.6437 m^3) #05(7.2169 m^3) #06(51.9208 m^3) #07(10.7253 m^3)

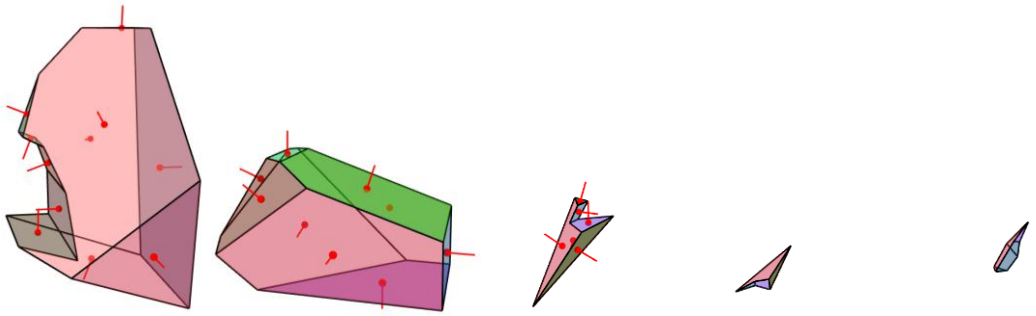

#08(22.2600 m^3) #09(13.5845m^3) #10(0.2751 m^3) #11(0.0948 m^3) #12(0.0532 m^3)

Figure 5- 8 Blocks with diverse shapes in tunnel

Since the surface of a tunnel excavation have different types: horseshoe-shaped tunnel, circular tunnel, square tunnel, etc., its intersection with a system of joints produces blocks with a curved face, or say concave block. In this example, a horseshoe-shaped tunnel is centered along the global *x* direction. The tunnel is located in rock containing three major discontinuities: 1) Dipping at 50^0 with a dip direction of 130^0; 2) Dipping at 45^0 with a dip direction of 45^0; 3) Dipping at 76^0 with a dip direction of 90^0. Several local tectonic joints are also distributed in the model.

Totally 12 blocks with diverse shapes are formed, including one key-block (Blk #11) in the roof of tunnel, other key-block (Blk #12) located at the side wall, as shown in the Fig. 5-11 and Fig. 5-12.

For clear demonstration, each block is shown in the perspective view with proper transparency, so that the details of each facet could be seen clearly. It is worth to note that the denotation "♂" from the loop center is along the average exterior normal direction, which helps to guarantee the complete description on each block. The random block generation algorithm could be referred to as (He and Ma, 2010). The volume of each block is provided by the 3-D simplex integration method. The total volume of rock mass is 277.4533m^3. The excavation volume of tunnel is 25.6507m^3.

Tunnel 3-D NMM modeling

Similarly, the current NMM program does not have the function to simulate crack propagation. The model in this example is divided into 12 discrete blocks by existent discontinuities directly.

Table 5- 2 Parameters for 3-D tunnel example

Feature	Item tested	Value
Rock mass	Unit weight (kN/m^3)	38.57
	Poisson's ratio	0.25
	Young's modulus (GPa)	24.50
	In-situ principle stress (MPa)	-0.01
Discontinuity	Initial frictional angle (^{0})	59.00
	Cohesion (MPa)	0.0
	Tensile strength (MPa)	0.0
Analysis parameters	Displacement-allowed ratio	0.003
	Maximum time increment (s)	0.001
	Normal contact spring stiffness (MN/m)	320.00
	Total time steps	10000

In order to present the compatibility between NMM and DDA, the whole model has been placed into a giant tetrahedral manifold pattern (MP). From some point of view (Ma et al., 2010), it is also a 3-D DDA example. Except the top face, other 5 faces are fixed in the model. The model has unified rock mass parameters and uniform property of discontinuities inside, listed in Table 5-2. Under only gravitational loading, some of such discrete blocks are unstable.

Tunnel Results Analysis

Unfortunately, current version of 3-D NMM has not yet included bolt model, therefore it could not further discuss on the enforcement scheme. If the tunnel is excavated without any support, it could keep stable against gravity (g = 9.8 m/s^2) under the friction resistant (59^0) and in-situ principle stress only. Gradually reduce the value of friction angle, there are two potential falling blocks in the example, indexed with Blk #11 and Blk #12. Obviously, the locations of these two key blocks are different, and their surrounding geometrical conditions are also different. Hence, they require different friction angles to keep their original locations. Table 5-3 gives their critical friction angles for both two key blocks.

Table 5- 3 Critical friction angle for two key-blocks in tunnel

	Roof Blk#11	Side Wall Blk#12
3-D NMM solution	11.107^0	17.645^0

With surrounding blocks hidden(Block#1 is hidden) for better viewing, Fig. 5-13 ~ Fig. 5-15 give the close-up view of the possible detached key-blocks. Unexpectedly, the key block #12, located at the side of tunnel, is in a situation relating less-stable compared with the roof block #11. As in the Table 5-3, roof block stands still when side block starts to be detached under the friction angle 15.50^0 (as shown in Fig. 5-14).

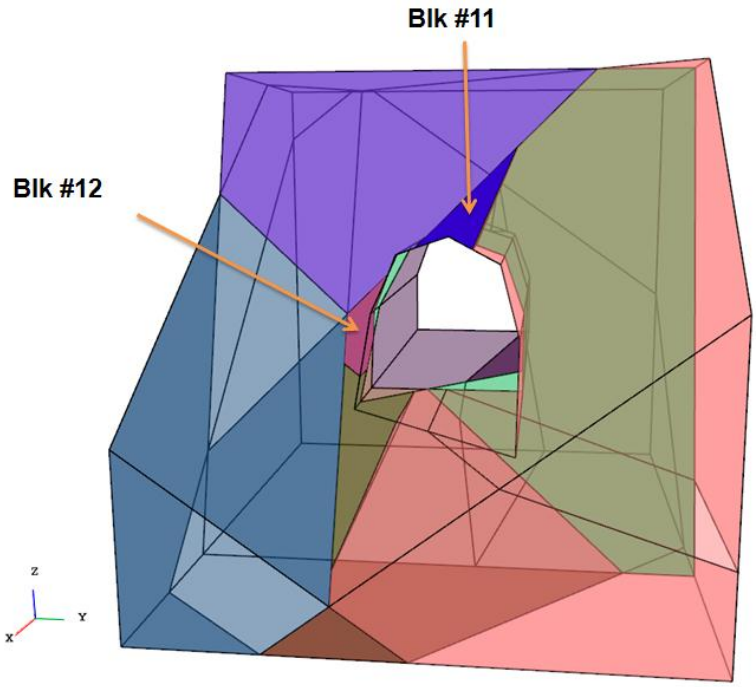

Figure 5- 9 Close-up view of the key-blocks

Even though the free surface of the roof block is at the bottom and more effective gravity components acting on, it is found that surrounding rock blocks contributes much more normal component of pressure to the roof block as the narrow shape of the block. These three contact faces are in relative embracing position. Conversely, only two faces on the side block are pairing with a relatively large angle, and embedded depth of the side block is much shallow. Therefore, less normal force perpendicular to contact face can be obtained, which lead to insufficient frictional resistance.

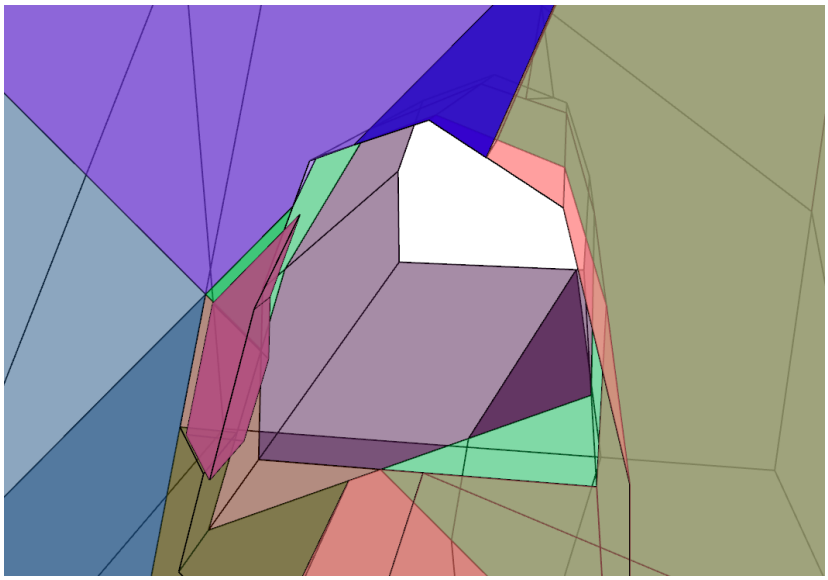

Figure 5- 10 Failure of key block located at the side wall

Figure 5-15 gives rock tunnel failure process with a frictional angle of 8^{o}, which means that both two key blocks in this tunnel model will be detached from the surrounding blocks and fall down to the bottom of tunnel.

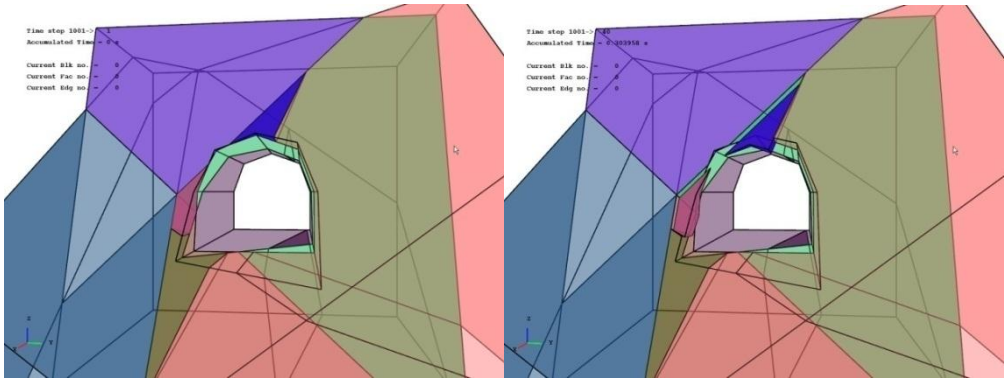

(a) 0.000s (b) 0.304s

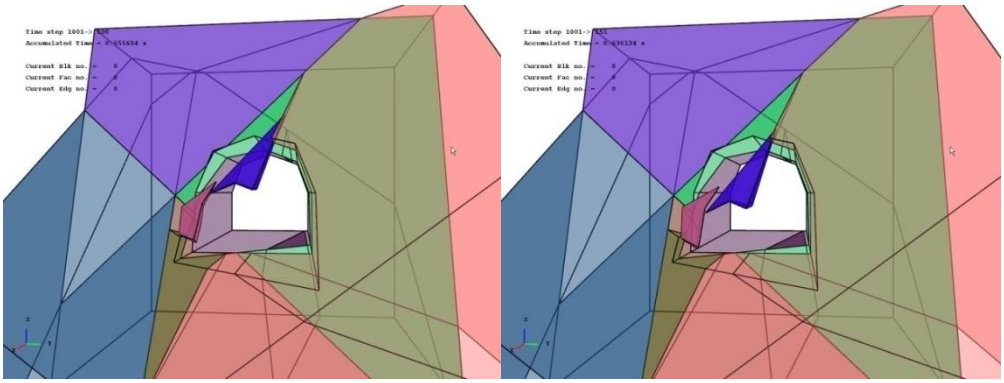

(c) 0.556s (d) 0.630s

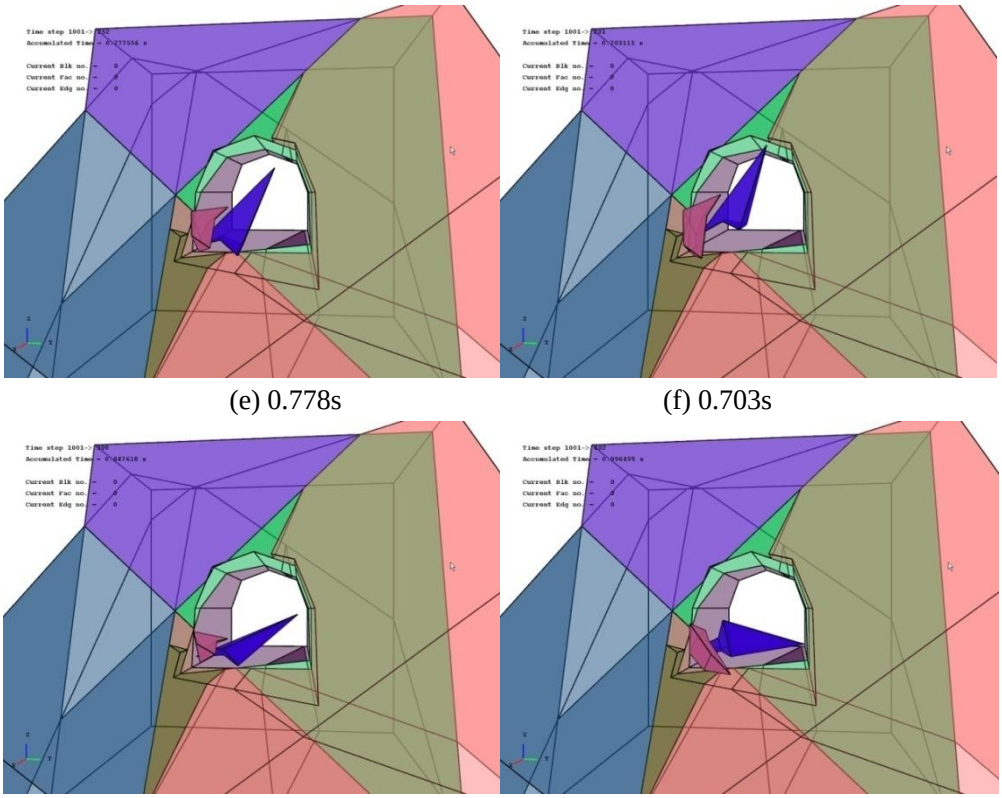

(e) 0.778s (f) 0.703s

(g) 0.848s (h) 0.996s

Figure 5- 11 Failure process of key-blocks in tunnel

The displacements of key blocks are monitored while the calculation is running. Fig. 5-16 plots the displacement history and indicated that the position of them is mainly moving downward. From the curvature change along the curve, we can also identify that block #11 will be completely detached from surrounding at time 0.776s. It later falls to the bottom of the tunnel at 1.172s. Similarly, side block #12 is detached at 0.709s, and falls to the bottom at 1.605s.

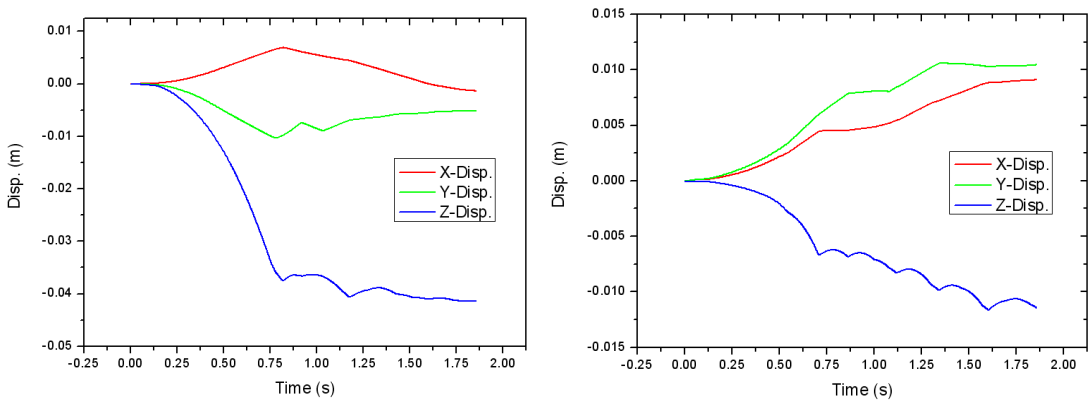

(a)Roof block #11 (b)Side block#12

Figure 5- 12 Displacement history of key blocks

This example focuses on the dynamic analysis to key block failure process with 3-D NMM and gain the critical friction angle for each key block. It fulfills to better test

the feasibility of developed 3-D NMM. Some facts in the example are discussed. 1) In this example, there are totally two key blocks which will be detached from its original location and fall to the bottom of the tunnel. The maximum collapsing volume is 0.148 m^3 under the setting condition, which will not crash as a whole. Enforcement scheme design should focus on how to prevent small block from falling. Generally speaking, lining and rock bolt should be enough for stabilization. 2) The program can simulate the whole process of collapse, and it can also get more detailed valuable information (including collapse time, collapse mode, volume velocity, etc.). 3) The example shows the complexity of the collapse process, which might not one-off happen. Some local collapse might predict that some of surrounding blocks are also at the edge of danger. It can also provide valuable suggestions on preventing secondary failure and tunnel obstacle release operation after accidents. 4) This example further verifies the stability of the contact algorithm and the potential ability to analyze the interactive contact among complex blocks. At the same time, 3-D NMM contact algorithm has been proved as a general contact logic, which should also work well in the platform of 3-D DDA.

Part 6: Concluding remarks

The thesis firstly manages to clarify the concepts to build a platform for discussing 3D NMM, which could not be found in previous studies. This has created a unified understanding to NMM, especially for geometric configuration of 3-D manifold pattern.

This thesis has also derived basic equations with proper numerical verifications and application examples, especially on 3D contact and modeling. A preliminary version of the 3D NMM has been developed. It has the ability to analyze both static and dynamic problem, armed with 3-D contact algorithm. Application examples show that the 3D NMM is accurate and suitable to rock slope/tunnel engineering problems. It opens a bright future for 3D NMM applications to practical engineering analysis.

In order to cover both continuous and discontinuous features of rock mass in rock engineering, it is required to describe irregular joint network in rock mass, to describe dynamical contact interaction in real time, to describe the changing process from continuous to discontinuous situation as crack initiation and propagation criteria, and to describe the underground water and seepage. This thesis aims to meet the first two requirements, and not yet the last two.

In other words, more works could be done to have better rock mass description, and to complete the description on the key features of rock masses (Not continuous, Not isotropic, Not homogeneous, Not linear, Not uniform, Mutli Physics). Further research could also make effort to focus on crack initiation and propagation criteria & underground water/seepage.

It is also meaningful to enhance dynamic analysis, such as Seismic loading analysis and underground earthquake-proof design, and explosive loading analysis and anti-detonation design.

Numerically, it could explore the direction of more element development, such as the development for 3-D shell, beam and string elements, and model of bolt and lining.

Selected Reference

Barton, N., Year, Shear Strength of Rockfill, Interfaces and Rock Joints, and their Points of Contact in Rock Dump Design. Rock Dumps Proceedings, Perth, Australian Centre for Geomechanics, Perth, 3-18, 5-6.

Benson, D.J. and Hallquist, J.O., 1990, A single surface contact algorithm for the post-buckling analysis of shell structures. Computer Methods in Applied Mechanics and Engineering, 78: 141-163.

Cheng, Y., Zhang, Y. and Chen, W., 2002, Wilson non‐conforming element in numerical manifold method. Communications in numerical methods in engineering, 18: 877-884.

Cundall, P.A., Year, A computer model for simulating progress large-scale movement in blocky rock system. Proceedings of the Symposium of the International Society of Rock Mechanics, France, 1-8.

Duncan, J. and Goodman, R., 1968, FINITE ELEMENT ANALYSES OF SLOPES IN JOINTED ROCK, Report, DTIC Document, 276 p.

Goodman, R., Taylor, R. and Brekke, T., 1968, A model for the mechanics of jointed rock. Journal of Soil Mechanics ASCE: 637-659.

Goodman, R.E., Shi, G.E. and Boyle, W.E., Year, Calculation of support for hard, jointed rock using the keyblock principle. Proceedings of 23th Symposium on Rock Mechanism, Berkeley, SME, New York, 883-898.

He, L. and Ma, G., 2010, Development of 3-D Numerical Manifold Method. International Journal of Computational Methods, 7: 107-129.

Itasca Conculting Group, I., 2003, 3 Dimensional Distinct Element Code-Theory and Background, Version 3.0, Report

Li, S., Cheng, Y. and Wu, Y.F., 2005, Numerical manifold method based on the method of weighted residuals. Computational mechanics, 35: 470-480.

Ma, G., An, X. and He, L., 2010, THE NUMERICAL MANIFOLD METHOD: A REVIEW. International Journal of Computational Methods, 7: 1-32.

SANCIO, R.T. and GOODMAN, R.E., 1979, Analysis of the stability of slopes in weathered rocks, University of California, Berkeley

Shi, G., 1988, Discontinuous deformation analysis: a new numerical model for the statics and dynamics of block systems, University of California, Berkeley, Berkeley

Shi, G., Year, Simplex integration for manifold method, FEM, DDA and analytical analysis. Proceeding of first International Forum on Discontinuous Deformation Analysis (DDA) and Simulations of Discontinuous Media, Albuquerque, NM, Mexico, 205-262.

Shi, G., Year, Numerical manifold method. Proceedings of the First International Conferences on Analysis of Discontinuous Deformation (ICADD-1), Chungli, Taiwan, 187-222.

Shi, G.H., Year, Manifold method of material analysis. Transaction of the 9th Army Conference on Applied Mathematics and Computing, Minneapolis, Minnesota, 57-76.